AGU PUBLICATIONS

JGR

Journal of Geophysical Research: Oceans

RESEARCH ARTICLE

10.1002/2013JC009632

Key Points:
- Quantification of the SSS variability processes in the Bay of Bengal
- Modeled SSS very consistent with in situ observations
- Specific role of vertical mixing evidenced in the seasonal budget of SSS

Correspondence to:
V. P. Akhil,
valiya.akhil@legos.obs-mip.fr

Citation:
Akhil, V. P., F. Durand, M. Lengaigne, J. Vialard, M. G. Keerthi, V. V. Gopalakrishna, C. Deltel, F. Papa, and C. de Boyer Montégut (2014), A modeling study of the processes of surface salinity seasonal cycle in the Bay of Bengal, *J. Geophys. Res. Oceans*, *119*, 3926–3947, doi:10.1002/2013JC009632.

Received 19 NOV 2013
Accepted 16 MAY 2014
Accepted article online 22 MAY 2014
Published online 24 JUN 2014

A modeling study of the processes of surface salinity seasonal cycle in the Bay of Bengal

V. P. Akhil[1], Fabien Durand[1], Matthieu Lengaigne[2,3], Jérôme Vialard[3], M. G. Keerthi[4], V. V. Gopalakrishna[2], Charles Deltel[3], Fabrice Papa[1,4], and Clément de Boyer Montégut[5]

[1]LEGOS, IRD/CNES/CNRS/UPS, Toulouse, France, [2]NIO, Goa, India, [3]LOCEAN, IPSL, Sorbonne Universités (UPMC, Univ Paris 06)/CNRS/IRD/MNHN, Paris, France, [4]Indo-French Cell for Water Sciences, Indian Institute of Science, Bangalore, India, [5]LOS, IFREMER, Plouzané, France

Abstract In response to the Indian Monsoon freshwater forcing, the Bay of Bengal exhibits a very strong seasonal cycle in sea surface salinity (SSS), especially near the mouths of the Ganges-Brahmaputra and along the east coast of India. In this paper, we use an eddy-permitting (~25 km resolution) regional ocean general circulation model simulation to quantify the processes responsible for this SSS seasonal cycle. Despite the absence of relaxation toward observations, the model reproduces the main features of the observed SSS seasonal cycle, with freshest water in the northeastern Bay, particularly during and after the monsoon. The model also displays an intense and shallow freshening signal in a narrow (~100 km wide) strip that hugs the east coast of India, from September to January, in good agreement with high-resolution measurements along two ships of opportunity lines. The mixed layer salt budget confirms that the strong freshening in the northern Bay during the monsoon results from the Ganges-Brahmaputra river discharge and from precipitation over the ocean. From September onward, the East India Coastal Current transports this freshwater southward along the east coast of India, reaching the southern tip of India in November. The surface freshening results in an enhanced vertical salinity gradient that increases salinity of the surface layer by vertical processes. Our results reveal that the erosion of the freshwater tongue along the east coast of India is not driven by northward horizontal advection, but by vertical processes that eventually overcome the freshening by southward advection and restore SSS to its premonsoon values. The salinity-stratified barrier layer hence only acts as a "barrier" for vertical heat fluxes, but is associated with intense vertical salt fluxes in the Bay of Bengal.

1. Introduction

The Indian peninsula splits the northern Indian Ocean into two semienclosed basins: the Arabian Sea (AS) to the west and the Bay of Bengal (BoB) to the east (Figure 1). The northern Indian Ocean is forced by annually reversing winds that blow from the southwest during the summer monsoon (May–September; Figure 1a) and from the northeast during the winter monsoon (November–March). This drives a seasonal reversal of most of the upper ocean currents north of 10°S, a unique feature among the three tropical oceans. The East India Coastal Current (EICC) flows along the western boundary of the BoB (Figures 2a–2d). This is a major oceanic current in the BoB, as it is responsible for most of the surface and thermocline water transport in this basin [*Schott and McCreary*, 2001; *Shankar et al*., 2002] and plays a key role in connecting the BoB with equatorial Indian ocean and AS [*Shankar et al*., 2002; *Durand et al*., 2009; *Shenoi*, 2010]. The EICC reverses seasonally, flowing northward before and during summer monsoon (Figures 2d and 2a) and southward after summer monsoon (Figures 2b and 2c). Only during November–December and March–April does the EICC form a continuous flow between the northern BoB and the southeastern coast of Sri Lanka. The EICC reversal precedes wind reversal by several months. This is due to the remote wind forcing from the equatorial Indian Ocean and eastern rim of the BoB, which propagates to the east coast of India in the form of coastal Kelvin waves [*Yu et al*., 1991; *McCreary et al*., 1993, 1996; *Shankar et al*., 1996]. This remote forcing, in conjunction with local wind forcing and intrinsic hydrodynamic instabilities, yields a rich spatio-temporal variability of the EICC [*Durand et al*., 2009; *Chen et al*., 2012; *Cheng et al*., 2013].

Although the BoB and AS are located in the same latitudinal belt and are both influenced by monsoons, the upper haline structure of these two basins differs markedly, with considerably fresher surface waters and more intense haline stratification in BoB (Figure 1b). The stronger humidity horizontal convergence results

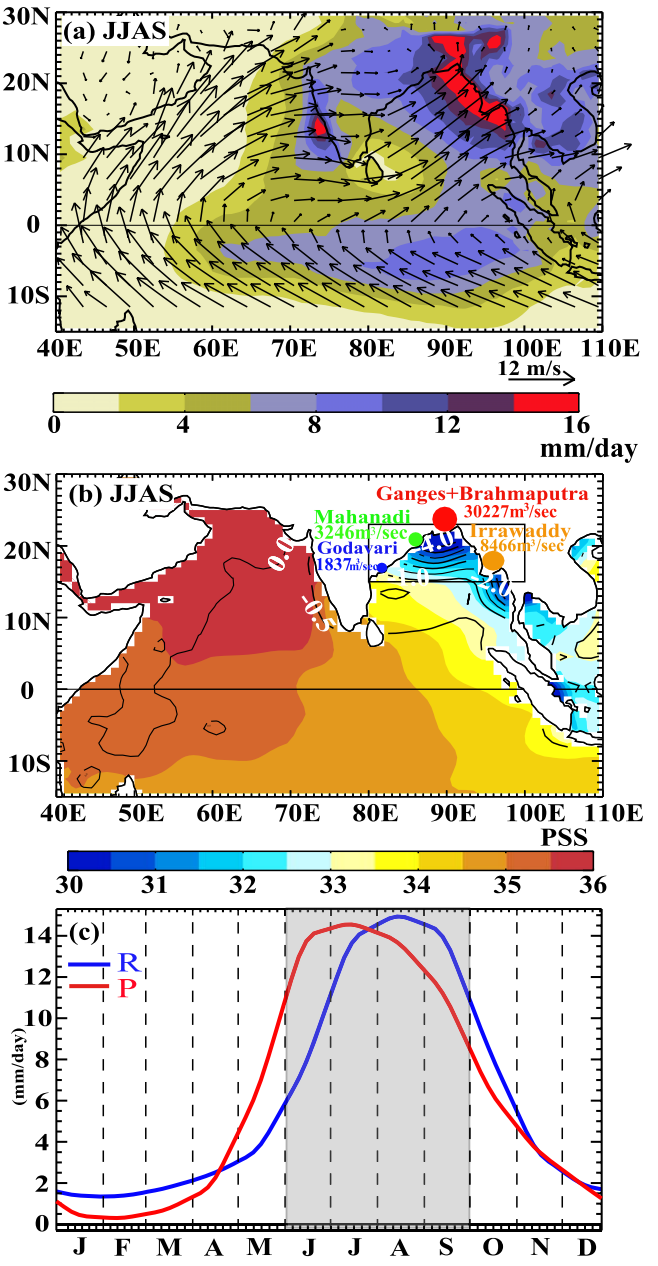

Figure 1. Summer (June–September) climatology of (a) GPCP rainfall (shaded) and 10 m QuikSCAT wind (vectors), (b) NIOA SSS (shaded), SSS minus salinity at 50 m depth (contours). The dots indicate the locations of major river mouths, the radius of each is proportional to the magnitude of mean fresh water outflow (m^3/s). The annual mean outflow is indicated, for each river. (c) Seasonal evolution of DFS4 rainfall in the BoB northward of 15°N (integrated over the ocean only) and of runoff from major rivers (Ganges-Brahmaputra, Irrawaddy, Mahanadi, and Godavari).

in much more intense rainfall over the BoB and surrounding continent (Figure 1a) than over the AS. Oceanic rainfall and continental runoffs (dominated by a handful of powerful rivers, i.e., Ganges, Brahmaputra, Irrawaddy, Mahanadi, and Godavari) contribute roughly equally to the total freshwater received by the BoB, north of 15°N (Figure 1c). These freshwater sources are located in the northern BoB (Figures 1a and 1b), resulting in lowest sea surface salinity (SSS) there (less than 33 units, in practical salinity scale). The low salinity surface waters lay above much saltier water (33–34.5 units, depending on the location) below 50 m, resulting in a sharp near-surface haline stratification (Figure 1b).

This very strong near-surface halocline potentially plays a strong role in maintaining the Northern Indian Ocean climate [*Shenoi et al.*, 2002]. It indeed strengthens the density stratification and usually results in a shallow mixed layer [*Mignot et al.*, 2007; *Thadathil et al.*, 2007; *Girishkumar et al.*, 2013]. Combined with a homogeneous thermal stratification, this often results in the formation of a barrier layer, the layer between the base of the mixed layer and the top of the thermocline [*Lukas and Lindstrom*, 1991]. This barrier layer prevents the vertical exchanges of momentum and heat between the upper mixed layer and the thermocline. This barrier layer is held responsible for the high sea surface temperature (SST) throughout the basin [*Shenoi et al.*, 2002; *de Boyer Montégut et al.*, 2007], which almost permanently remains above the 28°C threshold for deep atmospheric convection [*Gadgil*, 1984]. The salinity stratification also reduces the effects of storm-induced surface cooling in the BoB, which may in turn favor the intensification of tropical cyclones [*Sengupta et al.*, 2008; *Neetu et al.*, 2012; *Vincent et al.*, 2012]. It has also the potential to influence the amplitude of intraseasonal variability of the SST [*Vinayachandran et al.*, 2012] and biological productivity regimes [*Prasanna Kumar et al.*, 2002]. These strong impacts of haline stratification in the BoB call for a precise description and understanding of the SSS spatial structure and temporal variability within the Bay.

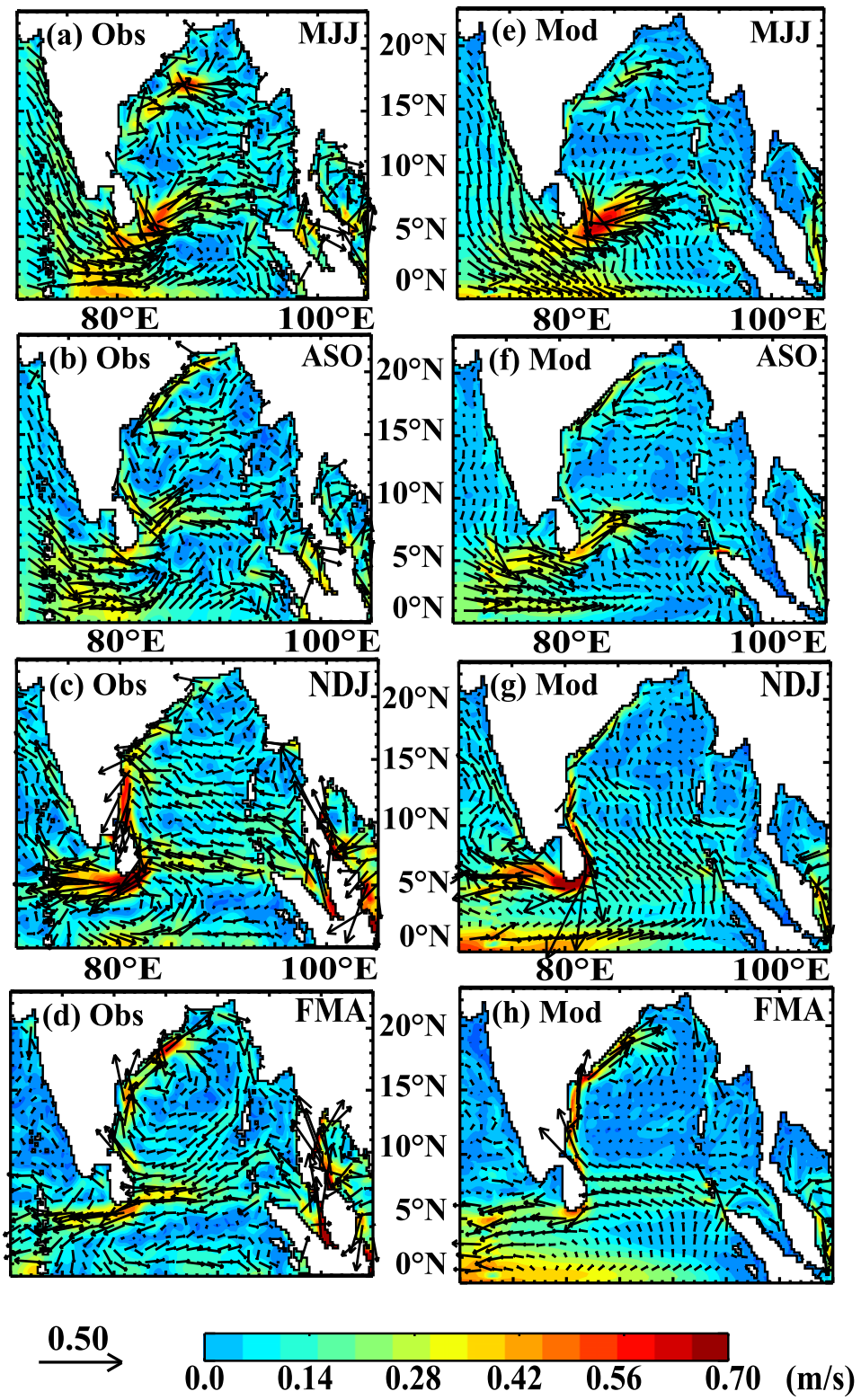

Figure 2. (left) Climatological surface current speed (color, m s^{-1}) and direction (vectors) in the BoB for (a) summer (MJJ), (b) autumn (ASO), (c) winter (NDJ), (d) spring (FMA) from GEKCO product. The climatology is computed over the 2002–2007 period. (right) Same for the model.

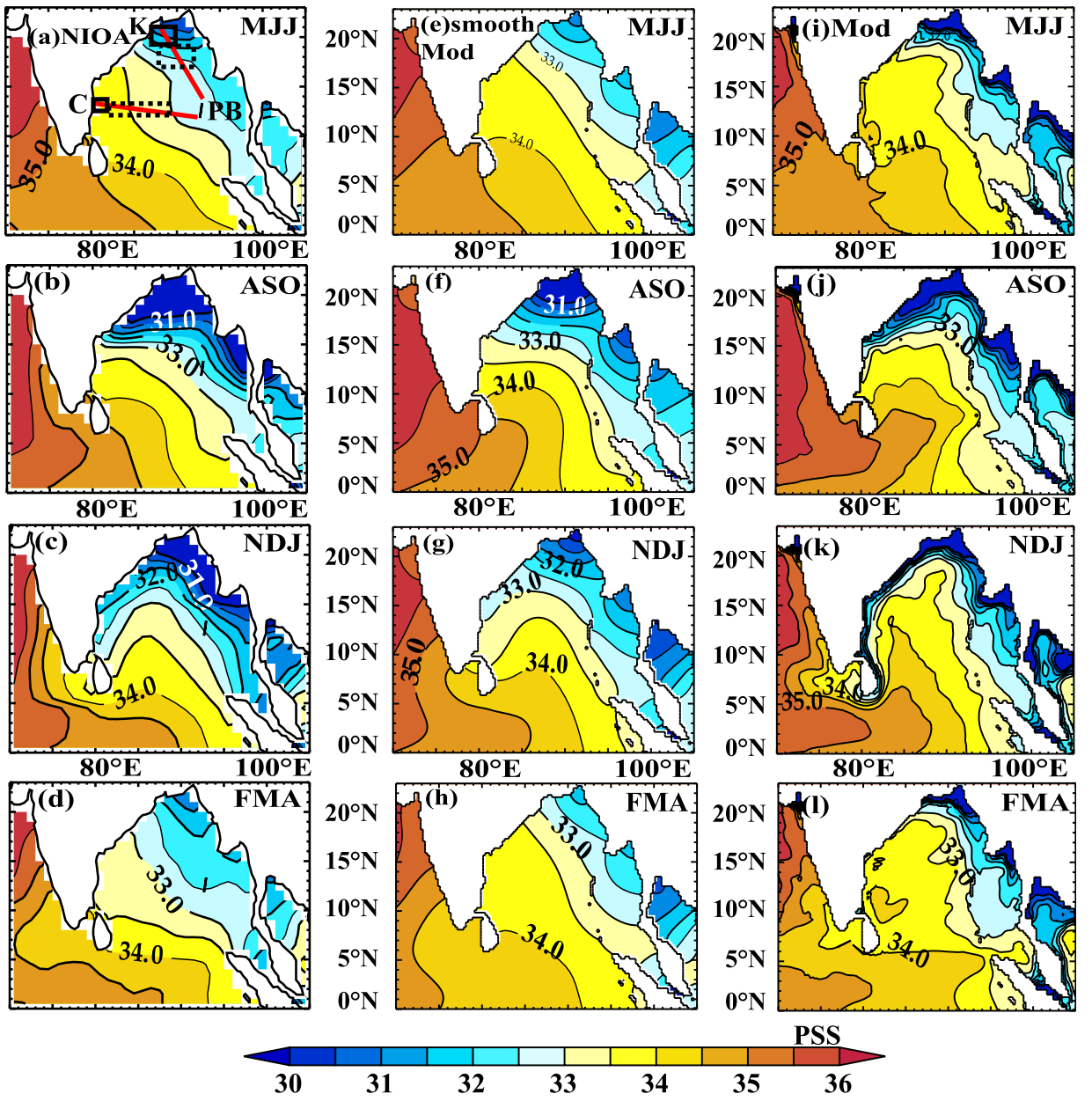

Figure 3. (left) Climatological SSS from NIOA [*Chatterjee et al.*, 2012] for (a) summer (MJJ), (b) autumn (ASO), (c) winter (NDJ), (d) spring (FMA). (middle) Same for the model climatology computed over the 2002–2007 period, in which a 444 km Gaussian smoothing has been applied, as in NIOA. (right) Model climatology again, but without smoothing. Salinity is given in practical salinity scale. The red lines in Figure 3a indicate the tracks of frequently repeated salinity measurements along two ship-of-opportunity lines: Chennai-Port Blair in the western Bay (C-PB) and Kolkata-Port Blair in the Northern Bay (K-PB). The box average of those data in the coastal (solid black) and offshore (black dashes) regions are compared with model values in Figure 4.

Observational studies describing the SSS within the BoB are mostly based on hydrographic measurements along dedicated cruises tracks and specific shipping lanes [*Shetye et al.*, 1991; *Murthy et al.*, 1992; *Shetye*, 1993; *Shetye et al.*, 1996; *Webster et al.*, 2002; *Babu et al.*, 2003; *Rao and Sivakumar*, 2003; *Vinayachandran and Kurian*, 2007] as well as on Array for Real-time Geostrophic Oceanography (ARGO) profilers data [e.g., *Vinayachandran et al.*, 2013; *Parampil et al.*, 2010]. *Rao and Sivakumar* [2003] reported a marked seasonal cycle of SSS, illustrated in Figure 3. During August–September–October, a tongue of low salinity (inferior to 30, in the practical salinity scale) water forms in the northeastern BoB (Figure 3b). This fresh pool spreads along both eastern and western boundaries of the basin in fall and early winter (Figure 3c). Subsequently, during late winter, the freshwater tongue weakens and retreats back to the northeastern Bay (Figure 3d). The freshwater supply varies strongly at seasonal timescale (Figure 1c), with about 70% of the annual inflow

(from precipitation and runoff) occurring during the summer monsoon north of 15°N. The observed freshening of the northern BoB in late summer (Figure 3b) clearly follows the seasonal maximum of precipitation in June and of river discharge in August (Figure 1c). While this role of freshwater forcing in the seasonal evolution of surface salinity has already been highlighted by several studies [e.g., *Shetye et al*., 1996, *Han et al*., 2001; *Sengupta et al*., 2006], the potential role of other processes (advection and vertical mixing in particular) is more difficult to evaluate from observations only. Earlier studies, however, proposed that the southward flowing EICC in November–December–January (Figure 2c) could play a role in conveying the freshwater plume southward along the western coast of India [*Shetye et al*., 1996; *Jensen*, 2001; *Rao and Sivakumar*, 2003].

Ship-based salinity observations are sparse in the Indian Ocean. While the ARGO program has considerably increased the number of temperature and salinity profiles in the central part of BoB since 2002, there is still a sparse coverage of the coastal regions. This leads the National Institute of Oceanography in Goa, India to develop a coastal salinity monitoring program at eight stations along the Indian coastline. Using this data, in combination with high-resolution data along an offshore transect, *Chaitanya et al*. [2014] demonstrated that there is a very intense freshening (up to 10 units in the northern Bay) in a narrow (∼50–100 km) coastal strip that quickly expands southward along the east Indian coast after the monsoon. This narrow freshening is not well captured by state-of-the-art climatologies [e.g., *Chatterjee et al*., 2012] due to both a poor data sampling in the coastal region and the 4° horizontal smoothing used in those climatologies. While it is difficult to derive a full salinity budget from observations, *Chaitanya et al*. [2014] analyses also suggest that the EICC plays a key role in the southward expansion of this narrow coastal freshwater strip after the monsoon, while other processes than advection are necessary to explain its decay during the following months.

While the improved in situ salinity observing network provides a better description of the SSS seasonal evolution within the Bay, it is, however, not yet sufficient to quantitatively assess all the processes that govern the seasonal SSS evolution. Numerical ocean circulation models have the distinct advantage of generating long time series of salinity at regular spatial and temporal intervals. With increasing accuracy of the forcing data, models are now able to simulate seasonal salinity variations with some realism. Several modeling studies provided some understanding of the impacts of the freshwater forcing (precipitation, evaporation, and runoff) on the upper BoB stratification and dynamics through sensitivity experiments [*Howden and Murtuggude*, 2001; *Han and McCreary*, 2001; *Han et al*., 2001; *Yu and McCreary*, 2004]. The common conclusion of these modeling studies is that river runoff, and not precipitation, is the dominant factor in freshening the northern part of the Bay during the southwest monsoon. *Han and McCreary* [2001], *Jensen* [2001], *Rao and Sivakumar* [2003], and *Nyadjro et al*. [2011] also identified lateral advection of low salinity waters from the northern BoB as the main driver of fresh water expansion along the east coast of India and into the AS during the monsoon. On the other hand, the eastern rim of the Bay appears to be a major export pathway of BoB freshwater toward the equator all year long [*Han and McCreary*, 2001; *Jensen*, 2001, 2003].

Most previous numerical modeling studies of the mechanisms of BoB SSS variability used a relaxation toward the observed surface salinity climatology. While this strategy allows keeping the surface salinity realistic [e.g., *Diansky et al*., 2006; *Wu et al*., 2007; *Sharma et al*., 2010; *Nyadjro et al*., 2011], the relaxation term will act to artificially compensate any error in the forcing or in the model physics. The relaxation term is sometimes strong in some locations of the BoB, so that it may be hazardous to infer robust conclusions about the mechanisms of SSS variability [*de Boyer Montégut*, 2005]. Some recent studies used coupled ocean-atmosphere models [*Vinayachandran and Nanjundiah*, 2009; *Seo et al*., 2009] with no relaxation, but precipitation in the atmospheric component of these coupled models is still insufficiently realistic to result in a satisfactory representation of BoB SSS variability.

The main objective of this study is to estimate the contributions of the processes that govern the SSS seasonal evolution in the BoB. To that end, we use an eddy-permitting regional ocean model with no relaxation to SSS observations that includes an online calculation of the terms contributing to the mixed layer salinity evolution. The rest of the paper is organized as follows. Section 2 briefly describes the modeling strategy and validation data. Section 3 validates the model to available observations. Section 4 discusses the processes that govern the SSS seasonal evolution, with a particular focus on the northern and western rim of the BoB where SSS variability is strongest. A discussion of our results is provided in Section 5.

2. Data and Methods

2.1. Model Description and Setup

The model configuration used in this study is based on the Nucleus of European Modeling of Ocean (NEMO) ocean general circulation modeling system [*Madec*, 2008], implemented in a regional Indian Ocean configuration (27°E–142°E, 33°S–30°N) described in *Vialard et al*. [2013]. It solves the primitive equations on a 1/4° horizontal grid with 46 vertical levels (vertical resolution ranging from 6 m at the surface to 250 m at the bottom, with 7 levels in the upper 50 m). Vertical mixing is modeled using a turbulent closure model that resolves a prognostic equation for the turbulent kinetic energy [*Blanke and Delecluse*, 1993]. The open boundaries are handled using a radiation-relaxation approach (following *Marchesiello et al*. [2001]), where we use the radiation condition to determine whether a boundary is passive (outward propagation) or active (inward propagation). The boundaries are constrained with a 150 day time-scale relaxation to 5 day average velocities, temperature, and salinity from an interannual global 1/4° simulation that has been carried out as part of the Drakkar project [*Drakkar Group*, 2007]. This global simulation has been extensively validated over the tropical Indian Ocean [*Keerthi et al*., 2013; *Nidheesh et al*., 2012].

The model is forced by interannually varying fluxes of momentum, heat, precipitation, evaporation, and runoff over January 2001–December 2007 from the Drakkar Forcing Set #4 (DFS4) described in *Brodeau et al*. [2010]. The starting point of DFS4 is the CORE data set developed by *Large and Yeager* [2004]. The CORE bulk formulae are used to compute latent and sensible heat fluxes, with surface atmospheric variables (air temperature, humidity, and winds at 10 m) from ERA40 reanalysis [*Uppala et al*., 2005] from 2000 to 2002, and European Center for Medium range Weather Forecast (ECMWF) analysis after 2002. Radiative fluxes are based on corrected International Satellite Cloud Climatology Project (ISCCP)-FD surface radiations [*Zhang et al*., 2004] while precipitation data are based on a blending of several satellite products, including two of the most widely used data sets: Global Precipitation Climatology Project (GPCP) [*Huffman et al*., 1997] and CPC Merged Analysis of Precipitation (CMAP) [*Xie and Arkin*, 1997]. All atmospheric fields are corrected to avoid temporal discontinuities and remove known biases (see *Brodeau et al*. [2010] for details). Following *Large and Danabasoglu* [2006] recommendations, turbulent fluxes are computed every 6 h while radiative fluxes are applied on a daily basis, with a linear interpolation to the model time step. We use monthly climatology of continental runoffs from *Dai and Trenberth* [2002], except for the Ganges-Brahmaputra river system for which we use altimetric-derived monthly interannual estimates [*Papa et al*., 2010]; this product gives us good confidence in the realism of the continental freshwater forcing of the model. We apply no relaxation to an observed SSS climatology in that experiment. The model is initialized from rest with World Ocean Atlas 2009 climatological temperature and salinity in January 2001, and only the January 2002–December 2007 period is analyzed in the present study.

Experiments using this model configuration and a similar forcing strategy (i.e., same as the above but with a climatological runoff everywhere and a relaxation to the observed SSS climatology) successfully reproduce intraseasonal [*Nisha et al*., 2013; *Vialard et al*., 2013] and interannual [*Praveen Kumar et al*., 2014] SST fluctuations in the Indian Ocean.

2.2. The Salt Budget in the Model

The model mixed layer depth (MLD) is defined as the depth where density is 0.01 kg m^{-3} higher than surface density. Such a small criterion allows the vertically averaged mixed layer salinity to be a good proxy of SSS [*de Boyer Montégut et al*., 2007]. In order to compute the ocean mixed layer (ML) salinity budget, the various terms contributing to salinity evolution are averaged over the ML online, stored as 5 day averages, and grouped as follows:

$$\partial_t\langle S\rangle = -\underbrace{\langle u\partial_x S + v\partial_y S\rangle}_{a} - \underbrace{\langle w\partial_z S\rangle}_{b} - \underbrace{\frac{1}{h}\frac{\partial h}{\partial t}\left(\langle S\rangle - S(z=h)\right)}_{c} + \underbrace{\frac{(k\partial_z S)(z=h)}{h}}_{d} + \underbrace{\frac{(E-P-R)S}{h}}_{e} + \underbrace{\langle D_l(S)\rangle}_{f} \tag{1}$$

where brackets denote the vertical average over the time-varying mixed layer depth h, S is the model salinity, (u, v, w) are the components of ocean currents, $D_l(S)$ the lateral diffusion operator, k the vertical diffusion

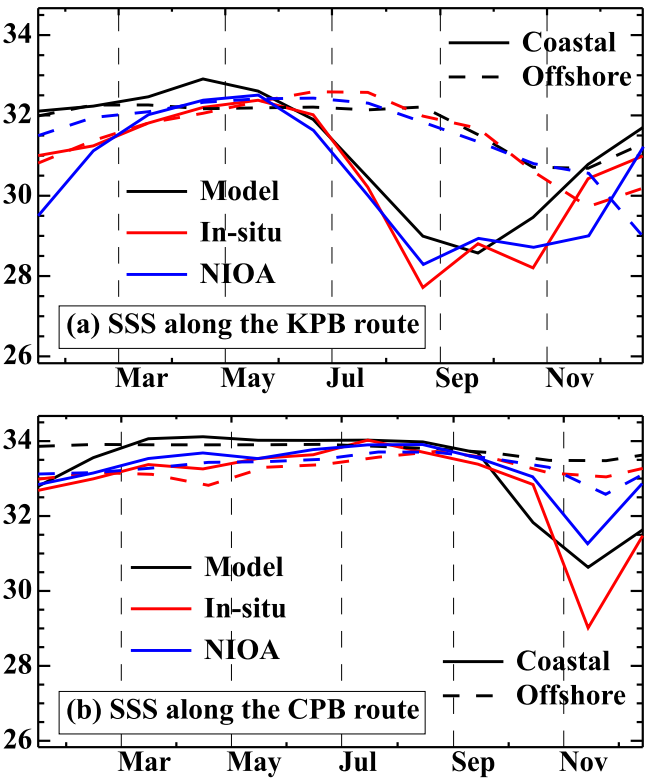

Figure 4. (a) Seasonal evolution of SSS from model (black), from ship-of-opportunity measurements (red) and from NIOA climatology (blue) along the K-PB route shown in Figure 3a. Solid lines are for the coastal box, dashes are for the offshore box. The boxes limits are shown in Figure 3a. (b) Same as Figure 4a, for the C-PB route.

coefficient, E is the evaporation, P the precipitation, and R the river runoff. The term (a) represents the horizontal advection, (b) the vertical advection, (c) is the entrainment, (d) the vertical diffusion through the mixed layer base, (e) is freshwater flux forcing of the mixed layer, and (f) is lateral diffusion.

We will use this salinity budget calculation to infer the respective contributions of these processes to the seasonal SSS evolution in the BoB. The term (f) for lateral diffusion is negligible as shall be seen in the following. The terms (b), (c), and (d) are grouped together in a vertical processes term. Our analyses will thus focus on identifying the relative influences of vertical processes ($b + c + d$), surface freshwater forcing (e), and horizontal advection (a).

2.3. Validation Data Sets

The model SSS is validated against the recent North Indian Ocean Atlas (NIOA) SSS climatology provided by *Chatterjee et al*. [2012]. This 1° by 1° monthly climatology includes all the data from the World Ocean Database 2009 (WOD09) [*Locarnini et al*., 2010; *Antonov et al*., 2010], complemented with Conductivity-Temperature-Depth (CTD) stations from Indian oceanographic cruises. An objective analysis gridding procedure (similar to that of World Ocean Atlas 2009) allows to fill the spatial data gaps and to smooth out the space scales shorter than 4°. The inclusion of the Indian oceanographic cruises database in NIOA considerably improves the data coverage in the periphery of the BoB compared with WOD09, especially along its western boundary [*Chatterjee et al*., 2012].

The scarcity of salinity data in the BoB and the smoothing applied to NIOA climatology prevents a proper resolution of the SSS climatological cycle in coastal regions. We therefore also use repeated bottle measurements performed by passenger ships that ply between India and Andaman Islands (between Chennai and Port Blair, as well as between Kolkata and Port Blair; see tracks on Figure 3a), and adequately sample India coastal margins. The data set spans the September 2006–May 2011 period, with typically a monthly to bimonthly frequency (6–13 cruises per year). During each cruise, an on-board scientific observer collects surface seawater samples (bucket samples) every 50–100 km. The samples are subsequently analyzed for SSS following standard international procedures, using a Guild Line 8400 Autosal salinometer. This ensures a typical accuracy of SSS data of about 10^{-2} unit. This long-term observational program allows us to validate the details of the model behavior in the coastal region of the northern BoB.

We finally use the Geostrophic and Ekman Current Observatory (GEKCO) surface current product of *Sudre et al*. [2013] to assess the model circulation. In this product, surface current is estimated from a combination of the geostrophic flow (estimated from altimetry) and Ekman flow (estimated from scatterometer winds) at a spatial resolution of 0.25° from October 1992 to present. A complete validation against in situ Eulerian and Lagrangian current observations can be found in *Sudre et al*. [2013]. Comparison with currents estimates derived from surface displacements of Argo floats results in correlations between 0.6 and 0.8 in the

Northern Indian Ocean. The observed climatology has been computed over the same period as the model simulation, i.e., the 2002–2007 period.

3. Validation

Figure 2 shows the GEKCO (left) and modeled (right) seasonal climatology of surface ocean currents. During the monsoon onset (May–July), the EICC flows poleward in its central section, and equatorward to the South of 8°N (Figure 2a) in both the model and GEKCO. During the decay of summer monsoon winds (August–September–October), the EICC reverses in both data sets in the northwestern BoB and starts flowing equatorward there (Figure 2b). The EICC is strongest during November–December–January and appears as a continuous equatorward flow all along the east coasts of India and Sri Lanka, with velocity above 0.6 m s^{-1} in its southern portion (Figure 2c). There, it bends around the tip of Sri Lanka and flows into the southeastern AS. This continuous flow does not last long, and reverses in February–March–April north of 8°N, then forming the western arm of a basin-wide anticyclonic gyre (Figure 2d). Overall, the model surface circulation (Figures 2e–2h) successfully reproduces the observed temporal evolution. The model satisfactorily reproduces the timing of EICC reversals, in line with earlier coarser versions of NEMO [e.g., *Durand et al.*, 2011]. It must however be noted that the modeled velocities are slightly too weak, in particular in the northwestern basin before summer monsoon (Figure 2e) and along the east coast of India between Sri Lanka and 15°N where they are underestimated by about 30% in November–January (Figures 2c and 2g).

The observed SSS field displays a contrasted pattern, with fresh waters in the northeastern BoB, and saltier waters in the central and southern basin (Figure 3). This large-scale gradient exists all year, but is seasonally modulated. During the presummer monsoon season (May–June–July), surface waters with salinity below 31 are restricted to the far northeastern BoB (Figure 3a). With the progression of summer monsoon (August–September–October), the surface waters freshen in the northern part of the BoB, and the freshening expands southward (Figure 3b). This southward expansion is especially noticeable along the eastern and western boundaries of the BoB, with clear signatures along the East coast of India at 16°N and in the southeastern BoB. Further south, saltier water (in excess of 34) prevails in the southeastern AS and the southwestern BoB. In fall (November–December–January) the fresh waters expand further south along the east coast of India, down to the northern tip of Sri Lanka (Figure 3c). Wintertime (February–March–April) is characterized by a northward retreat of the fresh waters in the western half of the basin and a salinity increase in the northeastern part of the basin (Figure 3d). The seasonal evolution seen in NIOA product is generally consistent with the past literature [e.g., *Rao and Sivakumar*, 2003].

As was previously mentionned, the NIOA climatology uses a 4° Gaussian smoothing in order to overcome the sparseness of in situ observations. *Chaitanya et al.* [2014] suggest that this horizontal smoothing may blur small-scale structures such as the narrow postmonsoon freshwater strip they describe in their data set. In order to provide a consistent comparison between the NIOA climatology and the model, we have also applied a 4° Gaussian smoothing to the model (Figures 3e–3h). The unsmoothed model is shown in Figures 3i–3l. Overall, the smoothed model reproduces the main patterns of the observed SSS climatology, and in particular the contrast between saltier water to the southwest and fresher water to the northeast. It also reproduces satisfactorily the main features of the SSS seasonal cycle, with a freshening in the northern BoB in ASO (Figures 3b and 3f), an expansion of the freshwater along the east coast of India in NDJ (Figures 3c and 3g), and gradual increase of salinity during FMA (Figures 3d and 3h). The smoothed model is in very good agreement with the NIOA climatology in MJJ and FMA (less than 0.5 unit salt bias), but displays a salty bias of up to 1.5 unit in ASO and 2 units in NDJ in the coastal strip, North of 15°N (figure not shown). The unsmoothed model SSS climatology displays much more intense gradients between freshest coastal waters and offshore saltier waters (Figures 3i–3l). In particular, it displays a narrow freshwater tongue hugging the east coast of India in NDJ, similar to the one described from observations by *Chaitanya et al.* [2014]. The realism of this narrow coastal freshwater strip is difficult to assess from a comparison with the smooth NIOA climatology. One way to address this issue is to perform a comparison to the high-resolution SSS sections harvested in the coastal region along the two ship tracks shown on Figure 3a.

Figure 4 shows the seasonal evolution of SSS in the coastal region (plain lines) near Kolkata at 21°N, 87°E (Figure 4a) and near Chennai at 13°N, 81°E (Figure 4b), along with the corresponding evolution further offshore (dashed lines), for the ship-borne observations (red), for the model (black), and for the NIOA

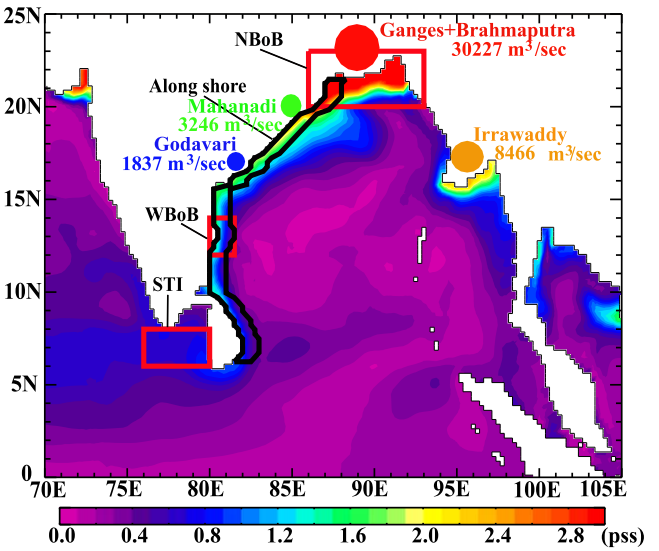

Figure 5. Standard deviation of the model's SSS monthly mean seasonal cycle. The red boxes feature the limits of the regions discussed in section 4: NBoB (86°E–93°E; 20°N–23°N), WBoB (80°E–81.5°E; 12°N–14°N), and STI (76°E–80°E; 6°N–8°N); the black line delineates the coastal strip box (extending 1° eastward from the western boundary). The major rivers mouths shown in Figure 1 are repeated here, for convenience.

climatology (blue). The observations and NIOA climatology both display a freshening of the Northern coastal BoB during the summer monsoon, a persistence of the freshwaters until November, followed by a salinity increase during winter-spring (Figure 4a). The southwestern coastal basin displays a similar evolution, but with a 3-month delay (Figure 4b). The model and NIOA climatology both reproduce the timing and amplitude of the coastal freshening near Kolkata (Figure 4a). Near Chennai, the high-resolution ship-borne data display a 5 units drop in coastal SSS from October to November (Figure 4b). The model and NIOA both reproduce the timing of this coastal freshening, but underestimate it (by 50% for NIOA and by 30% for the model). The fresh offset of the model compared to NIOA close to the coast is hence not due to model bias, but to the spatial smoothing in the NIOA climatology: the smoothed model is indeed ∼0.5–1 pss saltier than the climatology near Chennai at this season (Figures 4c and 4g).

The model displays a 1 unit salty bias of coastal SSS along the two ship tracks before monsoon season (April–May). Keeping in mind that the model SSS is not relaxed toward any observations, the reasonable agreement of the coastal SSS signal with the shipborne data is however quite remarkable. Overall, the comparison with the ship-of-opportunity data above suggests that, at least near Chennai and Kolkata, the model does not suffer from serious biases in the SSS and SSS gradient it simulates close to the coast. It also suggests that the model resolves the postmonsoon coastal freshening east of India slightly better than the NIOA climatology, in which spatial smoothing tends to damp this signal. We will discuss this issue further in the final section of the paper.

4. Processes of the SSS Seasonal Cycle Along the Indian Coastline

4.1. Overall Picture

Figure 5 shows the standard deviation of the model SSS climatology and highlights the regions of large seasonal SSS changes. As expected, the strongest SSS variability appears off the mouths of the major rivers (Ganges-Brahmaputra in the northern BoB, and Irrawaddy in the northern Andaman Sea) and—to a lesser degree—along the western boundary of the basin. In order to quantify the processes controlling seasonal SSS variations in the model, the temporal evolution of the various tendency terms of equation (1) are analyzed for a few areas, representative of the various regimes within the BoB. The geographical limits of the considered regions are highlighted in Figure 5. The Northern BoB (86°E–93°E; 20°N–23°N, hereafter NBoB) box is the region where most of the river freshwater enters the domain. The western BoB (80°E–81.5°E; 12°N–14°N, hereafter WBoB) box is a region typical of the western coastal basin, with relatively high SSS variability. The Southern tip of India (76°E–80°E; 6°N–8°N, hereafter STI) box is adjacent to the southwestern end of BoB, at the southernmost extremity of the tongue of strong SSS variability. Finally we also define an alongshore strip (black boundaries in Figure 5) spanning the entire western boundary, from 21°N to 6°N. This strip corresponds to the tongue of maximum SSS variability and will be used to display latitude-time sections of zonally averaged variables. Since the mixed layer depth is a critical element in our SSS budget method, we provide here a brief validation of the model to the observed mixed layer depth climatology of *de Boyer Montégut et al.* [2004] (Table 1). Although the model systematically overestimates the mixed layer

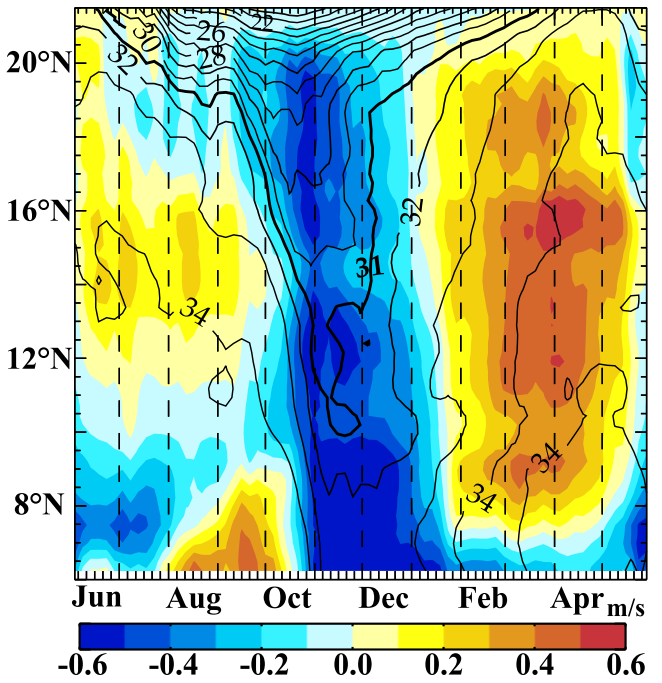

Figure 6. Latitude-time section of the model SSS (contours, pss) and alongshore current (shaded, negative values indicate southward current) seasonal cycle in the coastal strip box (limits defined by black lines in Figure 5) along east coast of Sri Lanka (6°N–10°N) and India (10°N–21°N).

depth deduced from observations, the resulting mean biases and root-mean-square errors are relatively small (a few meters, corresponding approximately to one model vertical level thickness). We will first discuss the seasonal evolution of mixed layer salinity budget along this alongshore strip. We will then focus on the three boxes (NBoB, WBoB, and STI) and investigate the mechanisms at stake for controlling SSS variability in each of those regions.

Figure 6 displays a latitude-time evolution of the modeled seasonal SSS and alongshore surface currents within the strip off the East coast of India. From June, SSS starts decreasing in the northernmost part of the BoB, reaching values as low as 18 in October. This freshening quickly migrates southward in September–October. By November, this fresh tongue reaches its southernmost limit, with salinity below 31 extending southward to 10°N. The 3 month delay of the seasonal freshening off Kolkata relative to that off Chennai (Figure 4) is explained by the southward migration of the freshwater front, from 20°N to about 10°N, at a speed of about 0.2 m s^{-1} (as inferred from the southward movement of the 31 isohaline). This fresh tongue considerably weakens in December–January, with a roughly simultaneous salinity increase in late November–early December throughout the 10°N–19°N portion of the coastal strip. Overlaying the time-latitude evolution of seasonal alongshore current (color) and SSS (contour) along the coastal strip (Figure 6) clearly illustrates that the southward migration of the freshwater front in September–October closely follows the current reversal (from poleward to equatorward) during this period. This suggests an active role of horizontal advection on the southward migration of the SSS front. The retreat of the fresh tongue, on the contrary, occurs in December in the western BoB, about 1 month before the current reversal (from equatorward to poleward), suggesting that alongshore advection is not responsible for the northward retreat of the SSS front. Figure 6 also shows a gradual erosion of the SSS minimum as the freshwater tongue progresses southward, from values of less than 20 units at 21°N, to about 31 units at 10°N 2 months later. This erosion is suggestive of mixing processes, occurring along the path of the freshwater mass. A more quantitative analysis of the various terms contributing to the SSS seasonal variations along this coastal strip is further provided in the next paragraph.

Figure 7a shows the latitude-time evolution of the total SSS tendency within the coastal strip. The most striking feature is the sharp freshening pattern, originating from the northern BoB in June–July, lasting until the end of September, and migrating southward from August to November. This freshening appears to be a subtle balance between three considerable larger terms: freshening by the atmospheric and continental freshwater flux (Figure 7b), freshening by the advection from horizontal circulation (Figure 7c), and salinity increase by vertical processes (Figure 7d). The freshening is initiated by continental runoff by major rivers (Ganges and Brahmaputra—henceforth GB—and Godavari mostly, with a lesser contribution of Mahanadi river) picking up in July, reaching their maximum in August, and decaying through October. Huge freshwater input occurs east of our coastal strip box limit as a combination of oceanic rainfall over the northeastern BoB in summer (Figure 1) and part of the GB discharge. This freshwater is advected westward by the

Table 1. Statistics of Observed Climatological MLD (m) and Model MLD (m) in the Boxes Shown in Figure 5[a]

Boxes	Bias	Rmsd	Mean OBS	Mean MOD
NBoB	−4.2	7.3	17.0	21.1
WBoB	−5.3	11.0	30.0	35.3
STI	−5.1	9.4	24.2	29.3

[a]NBoB (86°E–93°E; 20°N–23°N), WBoB (80°E–81.5°E; 12°N–14°N), and STI (76°E–80°E; 6°N–8°N).

northern extent of the cyclonic gyre centered on (90°E, 19°N) from August to October; this is followed by a period of southwestward EICC throughout the northern part of the domain (November–December–January), which sustains the advection of the freshwater (Figure 2). This explains the strong freshening through horizontal advection seen during this period everywhere to the North of 18°N (Figure 7c). Figure 7c also confirms the key role of horizontal advection in driving the southward migration of the fresh tongue suggested in the previous paragraph. The vertical processes (defined as the sum of vertical mixing, entrainment, and vertical advection) consistently act to counteract the freshening driven by freshwater forcing and/or horizontal advection (Figure 7d). This is particularly visible from June to December North of 19°N, as well as near the Godavari river mouth centered on 16°N, from July to October, where vertical processes completely counteract the freshening induced by the Godavari runoff. The following gradual salinity increase of this fresh tongue (reflected as the moderately positive total tendency term from November to January in Figure 7a) is then mostly explained by vertical processes, which remain strongly positive all along the pathway of the SSS minimum tongue.

4.2. Northern Bay of Bengal

The seasonal SSS evolution in the northernmost part of the domain (NBoB box) and its controlling processes are detailed in Figure 8. Consistent with what was seen in the northernmost part of the coastal strip (Figure 7), the total tendency term evolution results from a subtle balance between three considerably larger terms: a systematic mixed layer freshening through freshwater forcing flux and horizontal advection, and a systematic salinity increase through vertical processes (Figure 8b). The freshening tendency during the first half of the monsoon is dominated by the freshwater input, almost completely driven by G-B discharge (Figure 8e), with a maximum freshening in July. From August to October, the salt input into the mixed layer resulting from mixing surface fresh water with underlying saltier water is maximum (Figure 8d) and acts to counteract the freshening through freshwater input. From September onward, vertical processes overwhelm the combined freshening effect of freshwater forcing and horizontal advection terms and are responsible for the gradual SSS increase. The freshening effect of horizontal advection broadly mirrors the evolution of the zonal current (Figure 8c), with a largest SSS decrease induced in October–November when the zonal current carries the freshwaters westward from the mouths of G-B and from the area of strongest precipitation in the northeastern BoB.

While the timing of the horizontal advection and surface forcing is easy to understand from the seasonal cycle of rain, runoff, and currents, the timing of the vertical mixing term (that evolves in phase opposition with surface salinity; Figures 8a and 8b) deserves some explanation. As pointed out earlier, vertical mixing in the BoB mixes surface freshwater with underlying saltier water (i.e., it brings saltier water into the mixed layer). The effect of vertical mixing of subsurface water into the mixed layer is usually parameterized as $w_e(\langle S\rangle - S_{-h})$, where w_e is an entrainment speed (the result of vertical mixing by turbulence), $\langle S\rangle$ is the mixed layer average salinity, and S_{-h} is the salinity just below the mixed layer [e.g., *Niiler and Kraus*, 1977]. The vertical mixing term will thus increase as the salinity difference between the mixed layer and subsurface salinity increases. Figure 8d shows that the $\langle S\rangle - S_{-h}$ difference is dominated by changes in SSS (i.e., the subsurface salinity S_{-h} varies much less than the surface salinity $\langle S\rangle$). The vertical salinity gradient is hence large during the summer monsoon, when surface salinity is fresh, resulting in a stronger saltening under the effect of vertical mixing with underlying water.

The explanation above however neglects one factor, w_e (i.e., vertical mixing or turbulence at the bottom of the mixed layer) that is also affected by salinity stratification. The sharp vertical density stratification generated by massive monsoonal surface freshwater inflow is indeed usually believed to limit vertical exchanges between the surface layer and the deeper layers [e.g., *Shenoi et al.*, 2002; *Agarwal et al.*, 2012; *Thadathil et al.*, 2007]. In other words, salinity stratification $\langle S\rangle - S_{-h}$ has two opposite effects on the salinity vertical mixing term: on one hand, an increase of the salt flux into the mixed layer due to the entrainment of relatively saltier water, but on the other hand a decrease due to an inhibition of turbulence and hence of w_e. Figure 8d indicates that the first effect dominates, and Figure 9 allows understanding why. Figure 9

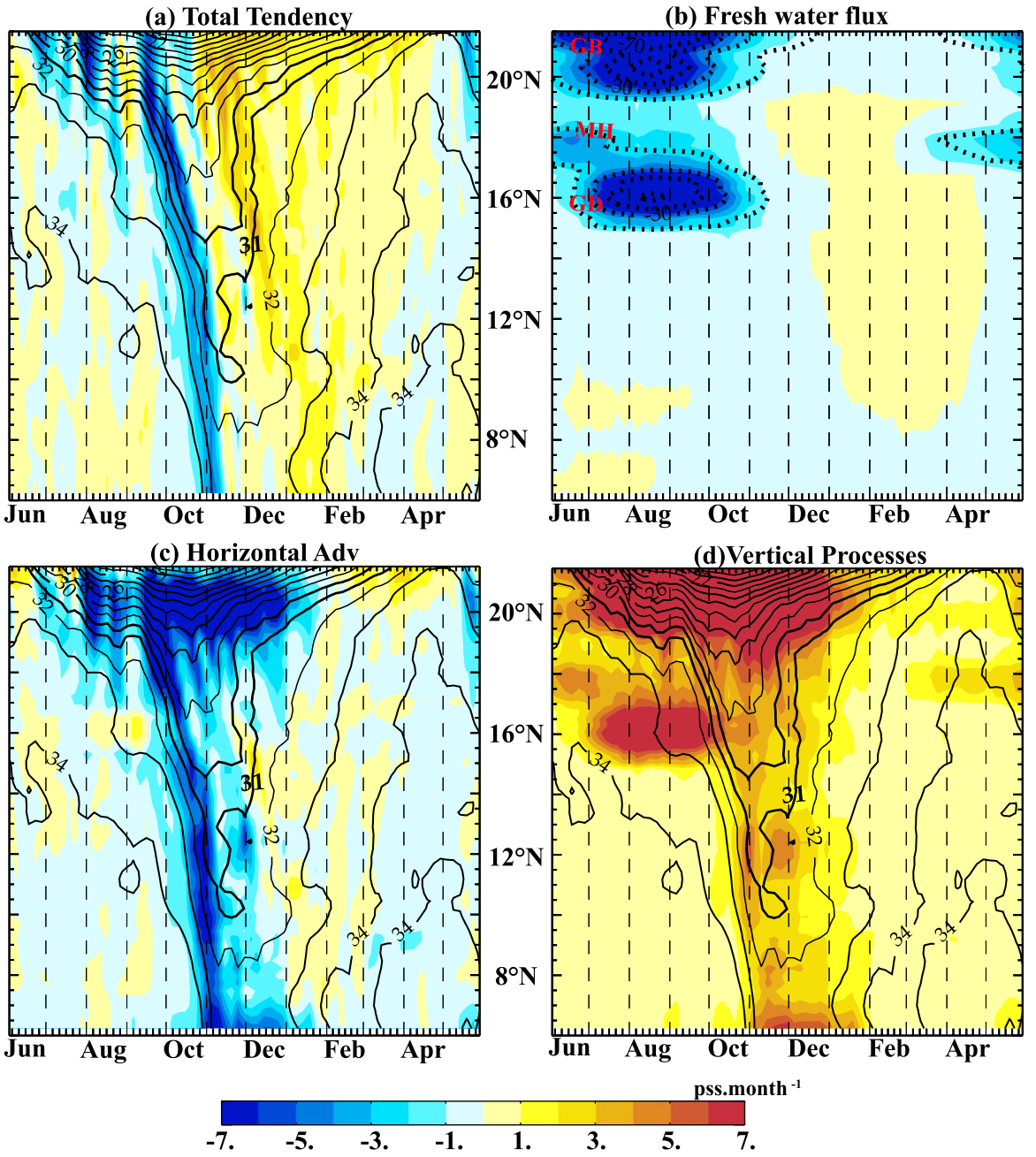

Figure 7. Latitude-time section of the model mixed layer salinity tendency terms (pss month^{-1}) mean seasonal cycle in the coastal strip box (limits shown in Figure 5) along east coast of Sri Lanka (6°N–10°N) and India (10°N–20°N): (a) total tendency, (b) freshwater forcing, (c) horizontal advection, and (d) vertical processes. Surface salinity (pss) is shown in contours in Figures 7a, 7c, and 7d. River runoffs (mm d^{-1}) are displayed in contours in Figure 7b, with GB, MH, and GD indicating, respectively, the mouths of Ganges Brahmaputra, Mahanadi, and Godavari rivers. See equation (1) for the formula of the terms plotted above.

provides the average temperature, salinity, and density profiles for the NBoB domain, during August–September–October (when vertical processes are maximum) and during February–March–April (when they are weaker). Vertical mixing is the result of transformation of turbulent kinetic energy into potential energy. Assuming heat and salt conservation and a perfectly homogeneous mixed layer (as in *Jourdain et al.* [2013]), we computed the energy required to increase surface salinity by 0.5 unit by vertical mixing of the mixed layer with underlying saltier water (see Appendix A for details). The 0.5 unit value corresponds to the typical salinity increase observed in the NBoB box over a week or so, over the October–April period (similar qualitative results are obtained for SSS increase ranging from 0.2 to 2). During August–October, it is only necessary to mix down

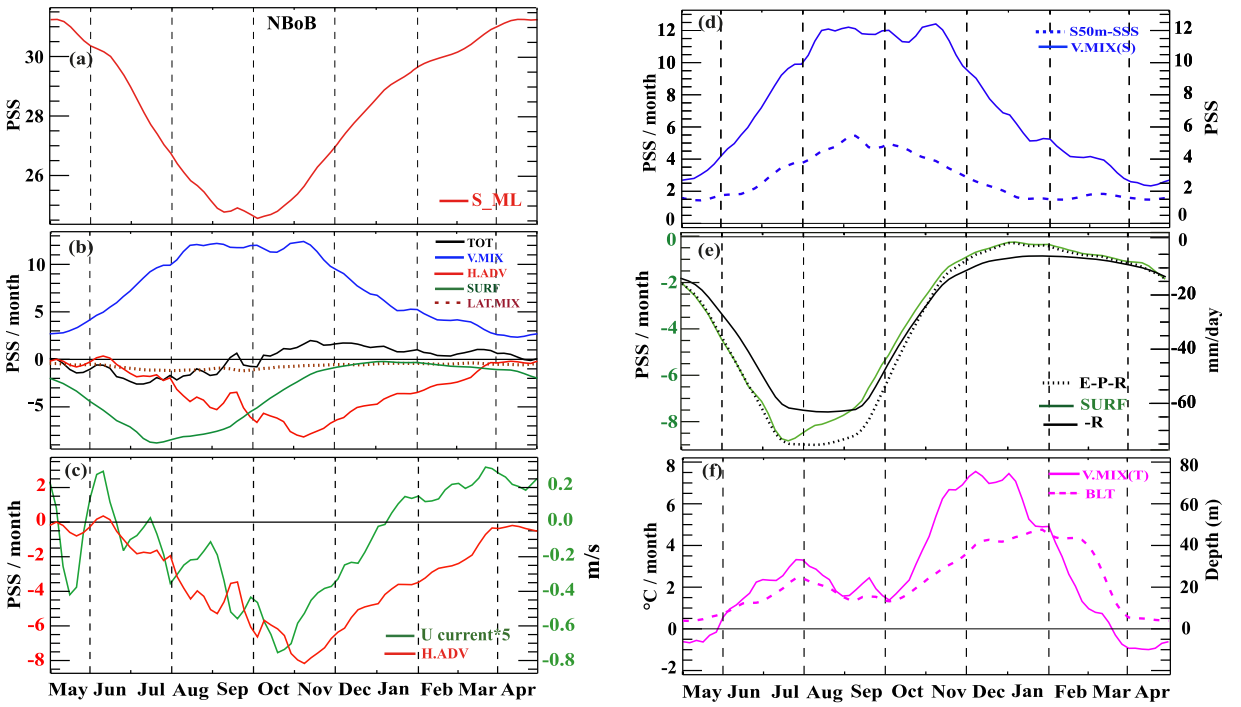

Figure 8. (a) Seasonal evolution of the average model mixed layer salinity over the NBoB box (limits shown in Figure 5). (b) Mixed layer salinity tendency terms (pss month^{-1}, horizontal advection in red, vertical processes in blue, surface freshwater forcing in green, lateral mixing in brown dashed line, and total tendency in black). (c) Horizontal advection term (red, pss month^{-1}) and zonal current (green, m s^{-1}). (d) Vertical mixing term (blue, pss month^{-1}) and salinity at 50 m depth minus SSS (blue dashed line, pss). (e) Freshwater forcing term (green, pss month $^{-1}$), freshwater flux E-P-R (black dashed line, mm d $^{-1}$), and river runoff (black line, mm d^{-1}). (f) Mixed layer temperature vertical mixing term (purple, °C month $^{-1}$) and barrier layer thickness (dashed purple, m).

to 13 m depth to yield a 0.5 surface salinity increase, because the upper ocean stratification is strong and shallow in that season. In contrast, it is necessary to mix the ocean down to 25 m depth in spring in order to obtain a similar salinity increase because of the weaker upper haline stratification in that season. The associated necessary energy to produce this mixing increases by a factor of 4 between the two seasons, from 133 J m^{-2} in summer to 572 J m^{-2} in spring. The idealized computation in Appendix A also indicates that, for a given salinity change, the requested energy decreases when the salinity stratification increases. This confirms that the inhibiting effect of salinity on turbulence is overwhelmed by the effect of the vertical salinity gradient on the salinity flux at the bottom of the mixed layer. A larger salinity stratification at the bottom of the mixed layer hence favors larger salinity increase by vertical mixing, consistent with what is seen in Figure 8d.

While vertical salinity stratification favors a stronger vertical salinity mixing, the effect is quite different on temperature. Because of the barrier layer, there is indeed a weak temperature gradient (or even a temperature inversion) between the BoB mixed layer and top of the thermocline, hence preventing mixing to cool the surface layer. This can be verified in our model by examining the vertical mixing term for temperature (equivalent of equation (1) for temperature, as was for example done in *de Boyer Montégut et al*. [2007] in the BoB, based on a similar model as ours). Figure 8f presents the modeled time series of the barrier layer thickness together with the vertical processes term of the mixed layer temperature budget. This term displays a completely different evolution from the salinity vertical processes term and remains positive most of the year. Because of the barrier layer effect (Figure 8f) and associated temperature inversion [*Thadathil et al*., 2002, 2007], mixing indeed systematically acts to warm the surface, except for a very brief 2 months period in April–May when the salinity stratification is weak. There is also a very clear modulation of the magnitude of the temperature vertical mixing term by the thickness of the barrier layer: thick barrier layers result in a larger warming of the surface, while thin barrier layer are associated with a weaker amplitude effect of vertical mixing. This contrasted impact of vertical mixing on mixed layer temperature and salinity may be summarized as follows: the barrier layer of the northern BoB enhances the mixed layer salinity increase by vertical processes, whereas it inhibits the mixed layer cooling. As the vertical gradient of salinity at the bottom of

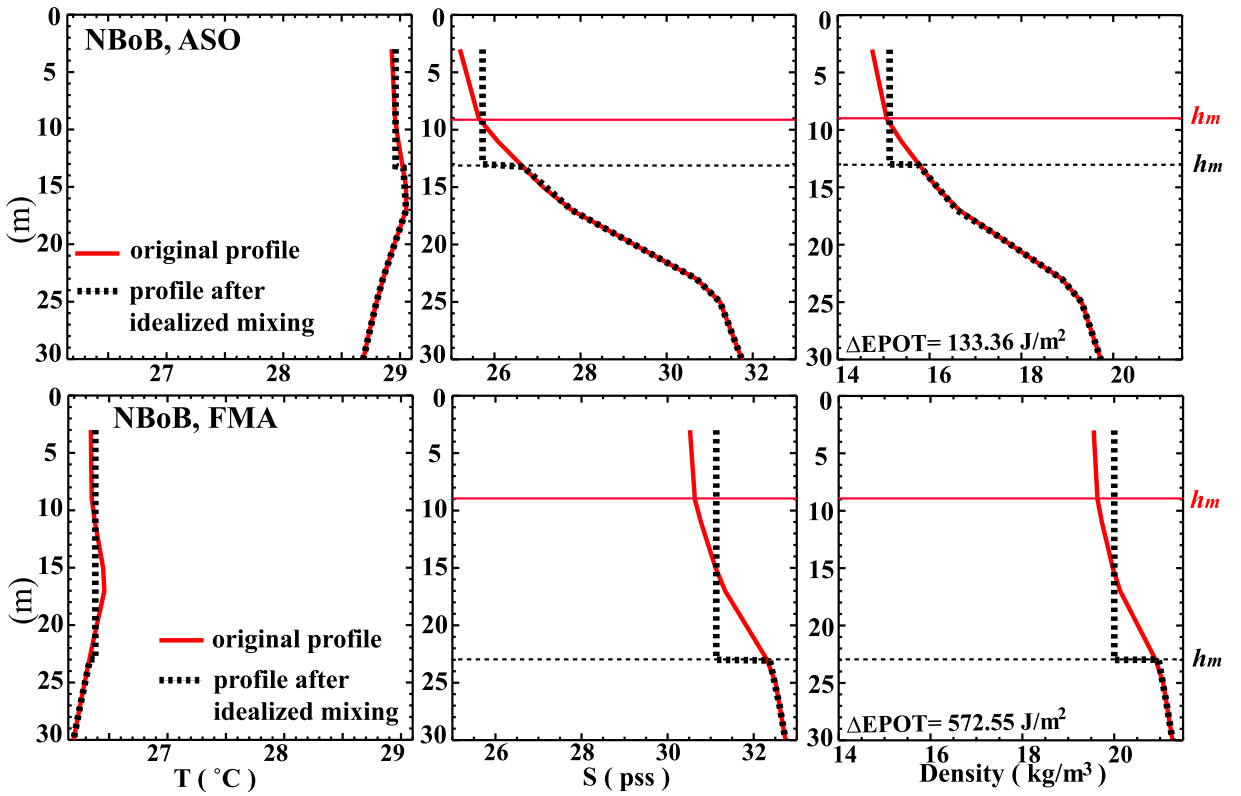

Figure 9. (top) Vertical profiles of model temperature, salinity, and density averaged over NBoB box (limits shown in Figure 5) during August–September–October (red line). Black dashed lines show idealized profiles that would yield a SSS rise of 0.5 unit under the effect of vertical mixing, assuming the conservation of salt and heat (see Appendix A for details). The difference in potential energy (ΔEPOT) of the water column before and after this mixing is indicated. Mixed layer depth (h_m) before mixing (in red) and after mixing (in black) is also indicated. (bottom) Same as top, for the February–March–April period.

the mixed layer is largely controlled by the mixed layer salinity (since subsurface variability of salinity is weaker than SSS variability), mixed layer salinity increase by vertical processes varies in phase with SSS.

In summary, freshwater forcing decreases mixed layer salinity in the NBoB during the summer monsoon. By September, the bulk of the freshwater has entered the ocean and advection picks up and spreads those low salinity water over the entire northern BoB. As salinity decreases, the vertical salinity gradient increases, and so does the surface salinity increase through vertical processes. In early October, surface salinity increase through vertical mixing overcomes the combined freshening through freshwater forcing flux and horizontal advection, and salinity starts increasing again. This surface salinity increase by vertical mixing lasts until the following monsoon onset (May).

4.3. The Western BoB and the Southern Tip of India

The WBoB box is located along the western boundary of the BoB, roughly halfway between the northern source of freshwater and the southern limit of the basin (Figure 5). SSS decreases abruptly from ∼34 in late September to 31.3 in early November (Figure 10a). This abrupt drop of 2.7 units is about twice smaller than the salinity decrease in the NBoB box between May and October (6.7 units). From early December, salinity starts increasing quickly and recovers its initial 34.0 value in late February. The basic equilibrium driving this seasonal evolution is somewhat simpler than for NBoB box, as it only involves two processes: horizontal advection that drives the freshening phase and vertical processes that induce the subsequent surface salinity increase (Figure 10b). The atmospheric forcing term is rather weak in the WBoB box (Figure 10b), and almost entirely driven by atmospheric fluxes (Figure 10e), with a freshening effect in October–November during the northeast monsoon, and evaporation from January to April. In contrast with the NBoB region, the total tendency term is of same order as the main individual terms. The horizontal advection is solely responsible for the September–October drop of SSS, as both the atmospheric freshwater flux and the

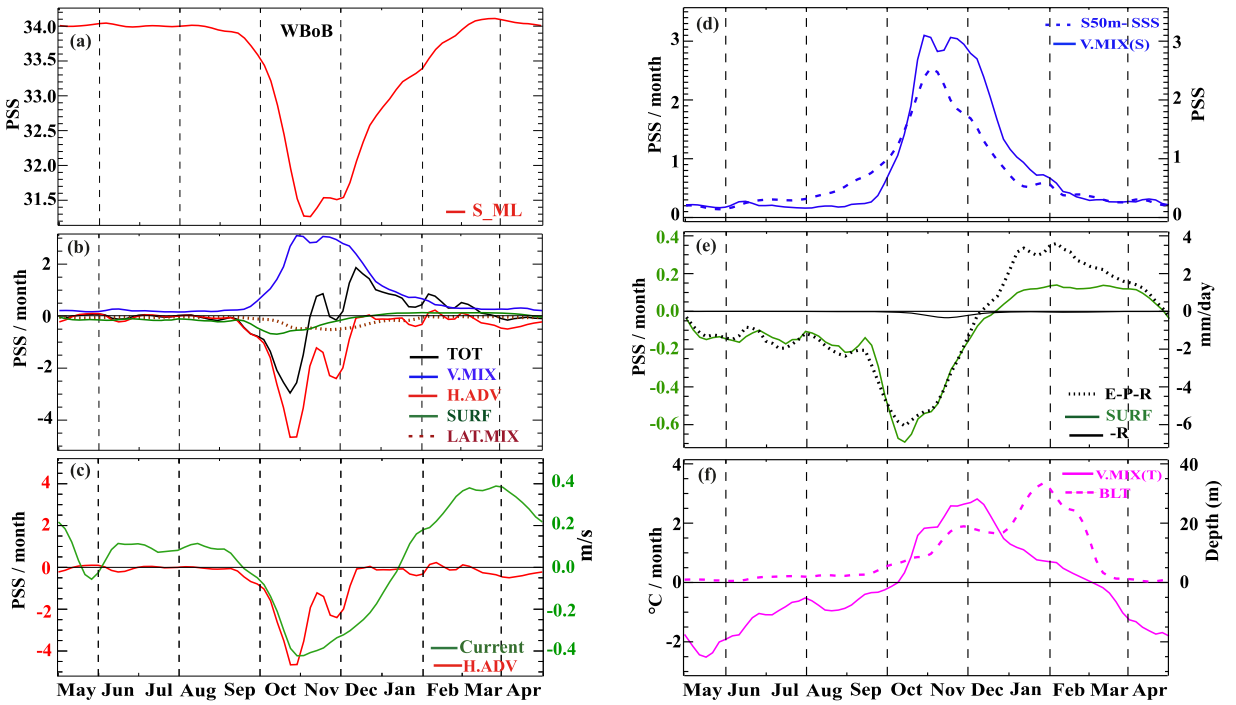

Figure 10. Same as Figure 8, for WBoB box (limits shown in Figure 5), except that the current (in green in Figure 10c) is here the alongshore current.

horizontal diffusion remain weak (Figure 10b). The horizontal advection terms pick up as soon as the southward flowing EICC enters the domain (Figure 10c). The two quantities evolve in concert up to December, with a weaker freshening effect as the southward flowing EICC decays in November–early December. Vertical processes start increasing in conjunction with the freshening onset in late September and then peak in November simultaneously with the maximum freshening (Figure 10b). The surface salinity increase simulated from early December onward is not driven by the advective term as the EICC is still flowing southward at that time but by vertical processes that overcome the advective freshening from early December onward. Moreover, advective processes never act to increase the SSS subsequently, because the coastal tongue of low salinity is already strongly eroded (Figure 6) by the time the EICC turns northward again from mid-January onward. Just like in the NBoB box, the seasonal evolution of vertical processes term is the mirror of the vertical gradient of salinity in the upper layers (Figure 10d). Given that subsurface salinity varies much less than SSS at seasonal timescales, the evolution of SSS appears here again as a good proxy of the evolution of the vertical processes term (with low SSS favoring a stronger salt flux into the mixed layer through vertical processes, and vice versa). As in the NBoB box, the vertical mixing of temperature behaves quite differently than the vertical mixing of salinity, with a cooling (warming) term in the absence (presence) of barrier layer (Figure 10f). To summarize, SSS along the west coast of India drops abruptly in fall when the southward flowing EICC brings freshwater from the northern BoB; the large salinity gradient between the surface and subsurface results in an enhanced surface salinity increase by vertical mixing, which then progressively erodes this freshening, and eventually restores the salinity to the premonsoon values.

The STI box, although not strictly located within the BoB, displays a similar behavior to the WBoB box: salinity drops suddenly in the postmonsoon season (from early November), and then increases gradually from January to August) (Figure 11a). Like in the WBoB box, the freshening phase is driven by horizontal advection, while vertical processes drive the subsequent surface salinity increase (Figure 11b). The atmospheric forcing term is also weaker than the other terms, and mostly associated with the northeast monsoon rains (Figure 11e). The magnitude of the seasonal SSS drop does not exceed 2 units, significantly less than in the WBoB box. The quasi-zonal Summer Monsoon Current (Figure 11c) flows westward from November to March and carries freshwaters from the BoB into the southeastern AS [*Shenoi et al.*, 1999; *Durand et al.*, 2007], through the STI region; this explains the evolution of horizontal advection in that box. Just like in the WBoB box,

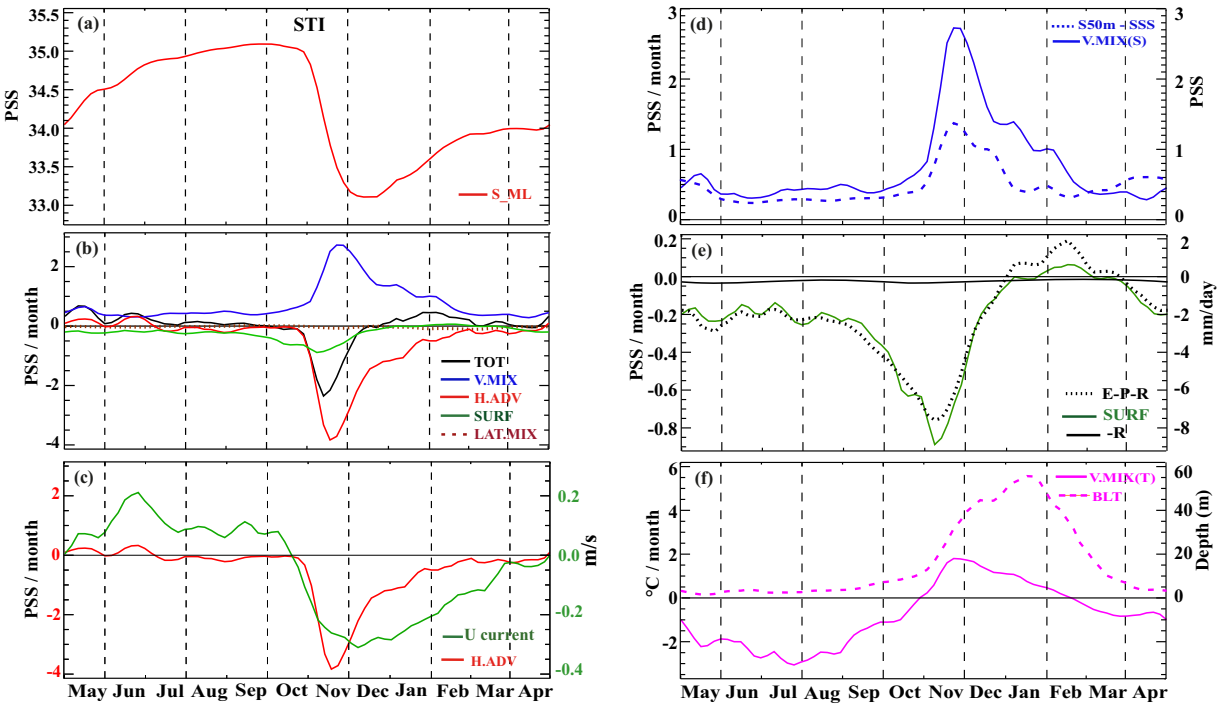

Figure 11. Same as Figure 8, for STI box (limits shown in Figure 5).

surface salinity increase by vertical processes counterbalances the freshening by horizontal advection. The evolution of the magnitude of vertical processes closely mirrors the evolution of vertical gradient of salinity in the upper layers, which evolves like SSS here as well (Figure 11d). On the other hand, the vertical mixing of temperature is rather related to the barrier layer thickness (Figure 11f), as in the WBoB box. One specific aspect of STI box, however, lies in the saltening effect of zonal advection at the beginning of summer monsoon (May and June; Figure 11d). At this time, the West India Coastal Current carries salty Arabian Sea water southward along the west coast of India, and feeds the eastward flowing Summer Monsoon Current [*Shankar et al.*, 2002]. The cumulated effect of this saltening advection throughout the spring and summer seasons is however much weaker than the saltening due to vertical mixing in the STI box (Figure 11c).

The contrasted impact of vertical processes on mixed layer salinity and temperature, observed in NBoB box and discussed in the previous section, is also seen in WBoB and STI boxes (Figures 10d and 11d). In October–February, the barrier layer is thick in the two boxes (Figures 10d and 11d). The barrier layer effect implies that this season when vertical processes act to increase mixed layer salinity is also the period when the vertical processes do not cool (and even warm) the mixed layer.

Overall, the NBoB, WBoB, and STI regions are quite homogeneous in their SSS variability mechanisms, with an inflow of freshwater in the northern BoB, and a subsequent horizontal transport along the western boundary of the BOB by the southward flowing EICC after the monsoon. This input of surface freshwater by EICC transport results in a larger vertical salinity stratification, which results in an increased surface saltening by vertical processes, which eventually restores mixed layer salinity to its premonsoon values.

5. Summary and Discussion

5.1. Summary

The objective of our study is to quantify the mechanisms that contribute to the SSS seasonal cycle in the BoB. To that end, we use an eddy-permitting (1/4°) regional simulation forced with altimeter-derived estimates of the river runoff for the Ganges and Brahmaputra (the two most important rivers), and no relaxation toward climatological observed SSS. Despite this absence of relaxation, our model adequately reproduces the main features of the observed SSS field, with freshest waters in the northeastern BoB,

especially during and after the summer monsoon. Our eddy-permitting model produces a narrow (∼100 km wide) coastal strip of freshwater along the coast of India after the southwest monsoon, which is not well resolved by existing observational SSS climatologies. This narrow coastal freshening is confirmed by relatively high-resolution (∼50 km and 2 month) salinity sections observed along two shipping lines between the east coast of India and central BoB. The relatively good agreement between the model and those observations encouraged us to use the model to quantify the dominant mechanisms of the SSS seasonal cycle. The BoB receives a large amount of freshwater from the Ganges and Brahmaputra and from oceanic precipitation during the summer monsoon that is the main cause for a large drop in SSS in the northernmost part of the BoB. From late September onward, this freshwater is advected southward by the EICC, as a thin tongue hugging the western boundary and that reaches the southeastern AS in early December. The salt influx into the BoB mixed layer (necessary to the long-term surface salinity equilibrium in this dilution basin) occurs prominently through vertical exchanges at the bottom of the mixed layer, during the monsoon and postmonsoon seasons. The magnitude of these vertical exchanges varies in space and time: strongest surface salinity increase tendencies occur when/where salinity stratification is strong. This is explained by the amplifying effect of salinity stratification on the vertical salt flux at the bottom of the mixed layer, which overwhelms the stabilizing effect of salinity. Strong salinity stratification has hence a very contrasted effect on temperature and salinity fluxes at the bottom of the mixed layer: on one hand, it favors the presence of barrier layer and shuts down entrainment cooling, but on the other hand it promotes surface salinity increase by vertical exchanges. Barrier layer hence only acts as a barrier for vertical heat fluxes, but allows considerable vertical freshwater/salinity fluxes.

5.2. Discussion

The most obvious limit of the current study is the observational coverage. The eastern half of the Bay is in particular undersampled compared to the western half [*Chatterjee et al*., 2012], making it hard to study SSS variations there. For example, our model displays a remarkable region of high SSS variability off the mouths of the Irrawaddy river (Figure 5). The SSS budget analysis in this area highlights mechanisms that are essentially similar to those in the NBoB region: surface freshwater (mostly from the river) is the dominant freshwater source; ocean circulation acts to spread it horizontally while vertical processes tend to increase the SSS. We did not display this analysis in the present paper, as the Andaman basin is completely devoid of SSS observations [*Chatterjee et al*., 2012] and we are hence not in a position to ascertain the validity of the model simulation there.

Our study agrees with previous modeling studies [*Howden and Murtugudde*, 2001; *Han and McCreary*, 2001; *Han et al*., 2001; *Yu and McCreary*, 2004] in designing river runoff, and not precipitation, as the dominant factor in freshening the northernmost part of the Bay during the southwest monsoon. *Han and McCreary* [2001], *Jensen* [2001], *Rao and Sivakumar* [2003], and *Nyadjro et al*. [2011] previously identified lateral advection of low salinity waters from the northern BoB as the main driver of fresh water expansion along the east coast of India after the monsoon. Our study agrees with these previous studies, but additionally provides a description of the trapping of the freshening close to the coast. This very narrow coastal freshening seen in the model is supported by ship-of-opportunity data. These data suggest that, at least at 21°N and 13°N, the model does not suffer from serious biases in the SSS and cross-shore SSS gradient it simulates close to the coast. The much broader coastal freshening seen in NIOA is most likely due to the scarcity of salinity data in the BoB and/or to the 4° smoothing applied during the objective analysis of *Chatterjee et al*. [2012]. Both salinity and current observations close to the coast are needed to better understand the magnitude, trapping scale, and timing of this freshening.

Contrary to what was suggested by *Shetye et al*. [1996] and *Vinayachandran and Nanjundiah* [2009], we find that the salt influx into the BoB mixed layer is not the result of horizontal advection from AS waters into the southwestern BoB. The salt influx into the BoB mixed layer (necessary to the long-term surface salinity equilibrium in this dilution basin) occurs prominently through vertical exchanges at the bottom of the mixed layer, during the monsoon and postmonsoon season, as initially suggested by *Shetye* [1993]. The magnitude of these vertical exchanges varies in space and time: strongest surface salinity increase by vertical processes occur when/where salinity stratification is strong. *Vinayachandran and Nanjundiah* [2009] reported a relatively moderate magnitude of the vertical processes in their SSS budget during the postmonsoon season. Their budget however neglected the vertical diffusion term (term (d) in equation (1)), which actually dominates the vertical processes in our model.

Although we identified vertical exchanges of salt as a key ingredient of the SSS budget, we are not in a position to quantitatively compare the balance from equation (1) in the model to an observed counterpart. Of course the relative realism of the model salinity and currents imply that the balance estimated from the model is valid at the first order. Our conclusions concerning the importance of vertical mixing for the long-term upper ocean salinity balance in the Bay of Bengal call for dedicated measurements of mixed layer processes, with microstructure measurements in order to estimate the vertical diffusivity in the upper oceanic layers, as in *Cuypers et al*. [2013] and *Moum et al*. [2013]. In addition, it may also be relevant to assess the robustness of our quantitative SSS budget in other state-of-the-art Ocean General Circulation Models (OGCMs), using different parameterizations of the vertical physics, horizontal resolution, and/or forcing data sets

The western rim of the BoB is an area of intense eddy activity [*Durand et al*., 2009]. A recent observational study indicates that those eddies may efficiently mix the coastal freshwater with offshore saltier water after the monsoon [*Hareesh Kumar et al*., 2013]. The ∼25 km resolution of our model is eddy-permitting, but not really eddy-resolving, and does not permit assessing the effect of the oceanic mesoscale circulation on the coastal freshwater strip. Refining the model resolution may also be a way to further improve the realism of our simulation. Our rather coarse 1/4° model indeed underestimates the EEIC by ∼30% on the southeastern coast of India in winter (Figures 2c and 2g), with a possible impact on the timing of the simulated coastal freshening. Using a higher ∼1/12° horizontal resolution would improve the simulated EICC, as discussed in *Benshila et al*. [2014]. Finally, increasing the vertical resolution in the upper layers (from 6 m to 1 m) may improve the representation of the very steep near-surface salinity stratification that is occasionally observed in the BoB [*Vinayachandran and Kurian*, 2007] and would allow to test the impact of the diurnal cycle of the buoyancy forcing fluxes on the salinity stratification. The modeling of the BoB (and in particular of its salinity structure) will undoubtedly benefit from higher resolution simulations in the future.

There are two interesting perspectives for our work. First, we found that the surface layer freshwater flux is balanced by a downward freshwater flux to the ocean's subsurface at the seasonal scale. Since the BoB is a semienclosed basin, this downward freshwater flux has to be evacuated by the oceanic subsurface circulation, i.e., on average, the subsurface horizontal flow into the Bay has to be saltier than the exit flow, in order to maintain the long-term balance. It will be interesting to study these subsurface freshwater fluxes in the future.

Due to the lack of data, very little is known about the interannual variation of SSS in BoB. The availability of remotely sensed surface salinity data from SMOS [*Mecklenburg et al*., 2012] and Aquarius [*Lagerloef et al*., 2008] satellites provides an interesting option for qualifying this interannual variability better. On the modeling front, the major limitation for representing interannual salinity variability by models was the lack of reliable continental freshwater forcing [*Vinayachandran and Nanjundiah*, 2009; *Durand et al*., 2011]. Now reliable interannual runoff estimates are available, at least for the dominant rivers of the BoB. This opens the way to study the mechanisms of SSS interannual variations of the BoB.

Appendix A: Energy Required for Increasing Surface Salinity by Vertical Mixing

Vertical mixing is the result of turbulent kinetic energy conversion into potential energy. In this appendix, we first summarize the approach of *Jourdain et al*. [2013], which allows computing the potential energy increase (i.e., required energy) to raise surface salinity by 0.5 units under the effect of vertical mixing. We then provide an analytical derivation of this necessary energy, in the idealized case of uniform salinity stratification, and no temperature stratification.

A1. Diagnostic of Necessary Mixing Energy From Model Profiles

Given a model temperature, salinity, and density (ρ_i) profile (like the red profiles in Figure 9), we want to compute how much energy is necessary to increase salinity by 0.5 units by vertical mixing. We will assume that the mixed layer is perfectly homogeneous after mixing, and heat and salt conservation.

An idealized "profile after mixing" is constructed (dotted profiles on Figure 9), assuming a homogeneous temperature and salinity down to a depth h_i (the homogeneous temperature and salinity in this profile are obtained by assuming heat and salt conservation over the depth h_i). (h_i) is increased iteratively until the difference in surface salinity between the original profile and idealized profile is 0.5 units. Once this "mixing depth" h_m has been obtained, the final profile density ρ_f is computed using the *Jacket and McDougall*

[1995] equation of state. The necessary energy per unit area that was needed for that mixing is computed from the potential energy change between the initial (red curves in Figure 9) and final (dotted curves in Figure 9) profiles using

$$\Delta E = \int_{hm}^{0} ((\rho_f - \rho_i) g z) dz$$

A2. Analytical Derivation in the Case of Uniform Salinity Stratification

In this section, we derive an analytical solution to the numerical calculation presented above for the simple case of an uniform salinity stratification, and negligible temperature effects (see Figure A1)

$$S(z) = SSS + bz,$$

where z is downward and b and SSS are constants.

We assume that density $\rho(z)$ is dominated by salinity changes, as is usually the case in the near-surface layer of the Bay of Bengal [e.g., *Shenoi et al.*, 2002]

$$\rho(z) = \rho_0[1 + \beta S(z)], where \beta > 0$$

Salt conservation gives

$$\int_{hm}^{0} (SSS + bz) dz = \int_{hm}^{0} S_f dz$$

$$SSS h_m + \frac{b h_m^2}{2} = S_f h_m$$

$$\frac{b h_m^2}{2} = h_m (S_f - SSS), where \quad (S_f - SSS) = \Delta S$$

$$\Delta S = \frac{bhm}{2}$$

The potential energy of the water column before mixing (E_B) is

$$\begin{aligned} E_B &= \int_{hm}^{0} (\rho g z) dz \\ &= \int_{hm}^{0} (\rho_o [1 + \beta (SSS + bz)] g z) dz \\ &= g \rho_0 \int_{hm}^{0} \left((1 + \beta SSS) z + \beta b z^2 \right) dz \\ &= -g \rho_0 \left[(1 + \beta SSS) \frac{h_m^2}{2} + \beta b \frac{h_m^3}{3} \right] \\ &= -\rho_0 g (1 + \beta SSS) \frac{h_m^2}{2} - \rho_0 g \beta b \frac{h_m^3}{3} \end{aligned}$$

The potential energy of the water column after mixing (E_A) is

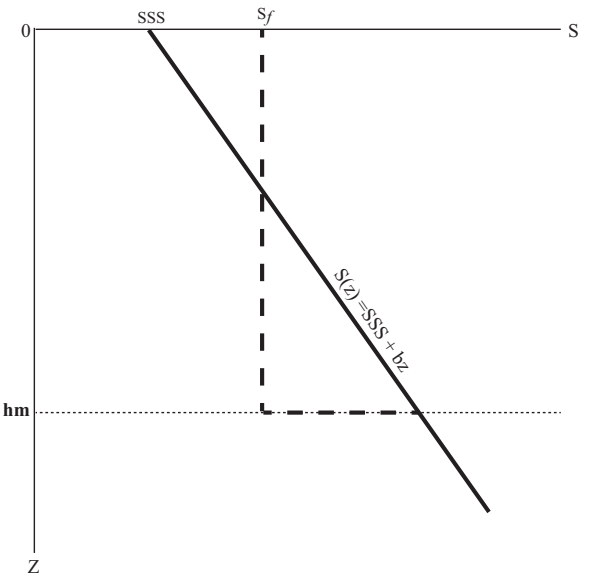

Figure A1. Idealized salinity profile used for the analytical computations. The thick black line corresponds to the idealized profile before mixing; the dashed line corresponds to the idealized profile after mixing.

$$E_A = \int_{hm}^{0} (\rho g z)dz = \int_{hm}^{0} (\rho_0 g(1+\beta S_f) g z)dz$$
$$= -\rho_0 g(1+\beta S_f)\frac{h_m^2}{2}$$

The required energy $\Delta E = E_A - E_B$ for increasing salinity by ΔS under the effect of mixing is

$$\Delta E = -\rho_0 g\beta S_f \frac{h_m^2}{2} + \rho_0 g\beta SSS\frac{h_m^2}{2} + \rho_0 g\beta b\frac{h_m^3}{3}$$
$$= \rho_0 g\beta \Delta S\frac{h_m^2}{2} + \rho_0 g\beta b\frac{h_m^3}{3}$$

and since $\Delta S = \frac{bh_m}{2}$

$$\Delta E = \frac{\rho_0 g\beta b h_m^3}{12} = \frac{2}{3}\rho_0 g\beta\frac{\Delta S^3}{b^2}$$
$$\Delta S = \sqrt[3]{\frac{3}{2}\frac{\Delta E}{\rho_0 \beta g}b^2}$$

In this idealized case, ΔS is proportional to $b^{2/3}$, i.e., for a given energy input ΔE, the amplitude of the salinity change induced by mixing increases with the salinity stratification. Salinity stratification has two effects on the surface salinity change. On one hand, a strong salinity stratification increases the salt flux into the mixed layer for a given mixed layer depth deepening. On the other hand, salinity stratification increases the static stability of the water column and tends to resist mixed layer deepening. The simple analytical calculation above suggests that the first effect dominates the second (i.e., larger vertical salinity stratification tends to favor large surface salinity changes through vertical mixing).

Acknowledgments

We acknowledge financial support by a TOSCA project from CNES, the French Space Agency. A.V.P. is funded through a PhD grant from CNES and IRD. We thank IRD for the financial support for the Indo-French collaboration on Indian Ocean research. In situ SSS samples are collected under support from Ministry of Earth Sciences (Government of India). The OGCM experiments were carried out on the cluster of IRD-Nouméa, New Caledonia. We thank Drakkar Group for providing the model boundary conditions. Thanks to Sébastien Masson for the SAXO plotting tools. This has NIO contribution number.

References

Agarwal, N., R. Sharma, A. Parekh, S. Basu, A. Sarkar, and V. Agarwal (2012), Argo observations of barrier layer in the tropical Indian Ocean, *J. Adv. Space Res.*, *50*, 642–654. doi:10.1016/j.asr.2012.05.021.

Antonov, J. I., D. Seidov, T. P. Boyer, R. A. Locarnini, A. V. Mishonov, H. E. Garcia, O. K. Baranova, M. M. Zweng, and D. R. Johnson (2010), *World Ocean Atlas 2009: Salinity*, vol. 2, edited by S. Levitus, pp. 184, U.S. Govt. Print. Off., Washington, D. C.

Babu, M. T., Y. V. B. Sarma, V. S. N. Murty, and P. Vethamony (2003), On the circulation in the Bay of Bengal during northern spring intermonsoon (March-April 1987), *Deep Sea Res., Part II*, *50*(5), 855–865.

Benshila, R., F. Durand, S. Masson, R. Bourdalle-Badie, C. de Boyer Montégut, F. Papa, and G. Madec (2014), The upper Bay of Bengal salinity structure in a high-resolution model, *Ocean Modell.*, *74*, 36–52.

Blanke, B., and P. Delecluse (1993), Variability of the tropical Atlantic Ocean simulated by a general circulation model with two different mixed layer physics, *J. Phys. Oceanogr.*, *23*, 1363–1388.

Brodeau, L., B. Barnier, A. M. Treguier, T. Penduff, and S. Gulev (2010), An ERA40-based atmospheric forcing for global ocean circulation models, *Ocean Modell.*, *31*(3–4), 88–104, doi:10.1016/j.ocemod.2009.10.005.

Chaitanya, A. V. S., M. Lengaigne, J. Vialard, V. V. Gopalakrishna, F. Durand, Ch. Krantikumar, V. Suneel, F. Papa, and M. Ravichandran (2014), Fishermen-operated salinity measurements reveal a "river in the sea" flowing along the east coast of India, *Bull. Am. Meterol. Soc.*, in press.

Chatterjee, A., D. Shankar, S. S. C. Shenoi, G. V. Reddy, G. S. Michael, M. Ravichandran, V. V. Gopalkrishna, E. P. Rama Rao, T. V. S. Udaya Bhaskar, and V. N. Sanjeevan (2012), A new atlas of temperature and salinity for the north Indian Ocean, *J. Earth Syst. Sci.*, *121*(3), 559–593, doi:10.1007/s12040-012-0191-9.

Chen, G., D. Wang, and Y. Hou (2012), The features and interannual variability mechanism of mesoscale eddies in the Bay of Bengal, *Cont. Shelf Res.*, *47*, 178–185.

Cheng, X., S. P. Xie, J. P. McCreary, Y. Qi, and Y. Du (2013), Intraseasonal variability of sea surface height over the Bay of Bengal, *J. Geophys. Res. Oceans*, *118*, 816–830, doi:10.1002/jgrc.20075.

Cuypers, Y., X. Le Vaillant, P. Bouruet-Aubertot, J. Vialard, and M. McPhaden (2013), Tropical storm-induced near inertial internal waves during the Cirene experiment: Energy fluxes and impact on vertical mixing, *J. Geophys. Res.*, *118*, 358–380, doi:10.1029/2012JC07881.

Dai, A., and K. E. Trenberth (2002), Estimates of freshwater discharge from continents: Latitudinal and seasonal variations, *J. Hydrometeorol.*, *3*, 660–687.

De Boyer Montégut, C. (2005), Couche mélangée océanique et bilan thermohalin de surface dans l'Océan Indien Nord, PhD thesis, 181 pp., Univ. of Paris VI, Paris. [Available at tel.archives-ouvertes.fr/docs/00/05/58/75/PDF/these_clem_pdf_edition_20051025.]

De Boyer Montégut, C., G. Madec, A. S. Fischer, A. Lazar, and D. Iudicone (2004), Mixed layer depth over the global ocean: An examination of profile data and a profile-based climatology, *J. Geophys. Res.*, *109*, C12003, doi:10.1029/2004JC002378.
De Boyer Montégut, C., J. Mignot, A. Lazard, and S. Cravatt (2007), Control of salinity on the mixed layer depth in the world ocean. Part I: General description, *J. Geophys. Res.*, *112*, C06011, doi:10.1029/2006JC003953.
Diansky, N. A., V. B. Zalesny, S. N. Moshonkin, and A. S. Rusakov (2006), High resolution modeling of the monsoon circulation in the Indian Ocean, *Oceanology*, Engl. Transl., no. 46, 608–628.
Drakkar Group (2007), Eddy-permitting ocean circulation hindcasts of past decades, *CLIVAR Exchanges 42*, *12*(3), 8–10.
Durand, F., D. Shankar, C. de Boyer Montegut, S. S. C. Shenoi, B. Blanke, and G. Madec (2007), Modeling the barrier-layer formation in the Southeastern Arabian Sea, *J. Clim.*, *20*, 2109–2120, doi:10.1175/JCLI4112.1.
Durand, F., D. Shankar, F. Birol, and S. S. C. Shenoi (2009), Spatiotemporal structure of the East India Coastal Current from satellite altimetry, *J. Geophys. Res.*, *114*, C02013, doi:10.1029/2008JC004807.
Durand, F., F. Papa, A. Rahman, and S. K. Bala (2011), Impact of Ganges–Brahmaputra interannual discharge variations on Bay of Bengal salinity, *J. Earth Syst. Sci.*, *120*(5), 859–872, doi:10.1007/s12040-011-0118-x.
Gadgil, S., P. V. Joseph, and N. V. Joshi (1984), Ocean–atmosphere coupling over monsoon regions, *Nature*, *312* 141–143.
Girishkumar, M. S., M. Ravichandran, and M. J. McPhaden (2013), Temperature inversions and their influence on the mixed layer heat budget during the winters of 2006–2007 and 2007–2008 in the Bay of Bengal, *J. Geophys. Res. Oceans*, *118*, 2426–2437, doi:10.1002/jgrc.20192.
Han, W., and J. P. McCreary (2001), Modeling salinity distribution in the Indian Ocean, *J. Geophys. Res.*, *106*, 859–877.
Han, W., J. P. McCreary, and K. E. Kohler (2001), Influence of precipitation minus evaporation and Bay of Bengal rivers on dynamics, thermodynamics, and mixed layer physics in the upper Indian Ocean, *J. Geophys. Res.*, *106*, 6895–6916.
Hareesh Kumar, P. V., B. Matthew, M. R. Ramesh Kumar, A. R. Rao, P. S. V. Jagadesh, K. G. Radhakrishnan, and T. N. Shyni (2013), 'Thermohaline front' off the east coast of India and its generating mechanism, *Ocean Dyn.*, *63*, 1175–1180, doi:10.1007/s10236-013-0652-y.
Howden, S. D., and R. Murtugudde (2001), Effects of river inputs into the Bay of Bengal, *J. Geophys. Res.*, *106*, 19,825–19,843.
Huffman, G., R. Adler, P. Arkin, A. Chang, R. Ferraro, R. Gruber, J. Janowiak, A. McNab, B. Rudolf, and U. Schneider (1997), The global precipitation climatology project (GPCP) combined precipitation data set, *Bull. Am. Meteorol. Soc.*, *78*, 5–20.
Jackett, D. R., and T. J. McDougall (1995), Minimal adjustment of hydrographic profiles to achieve static stability, *J. Atmos. Oceanic Technol.*, *12*, 381–389.
Jensen, T. G. (2001), Arabian Sea and Bay of Bengal exchange of salt and tracers in an ocean model, *Geophys. Res. Lett.*, *28*, 3967–3970.
Jensen, T. G. (2003), Cross-equatorial pathways of salt and tracers from the northern Indian Ocean: Modelling results, *Deep Sea Res., Part II*, *50*, 2111–2127.
Jourdain, N., M. Lengaigne, J. Vialard, G. Madec, C. Menkes, E. Vincent, S. Jullien, and B. Barnier (2013), Observation based estimates of surface cooling inhibition by heavy rainfall under tropical cyclones, *J. Phys. Oceanogr.*, *43*, 205–221, doi:10.1175/JPO-D-12–085.1.
Keerthi, M. G., M. Lengaigne, J. Vialard, C. de Boyer Montégut, and P. M. Muraleedharan (2013), Interannual variability of the Tropical Indian Ocean mixed layer depth, *Clim. Dyn.*, *40*, 743–759.
Lagerloef, G., F. R. Colomb, D. Le Vine, F. Wentz, S. Yueh, C. Ruf, J. Lilly, J. Gunn, Y. Chao, A. deCharon, G. Feldman, and C. Swift (2008), The Aquarius/SAC-D Mission: Designed to meet the salinity remote-sensing challenge, *Oceanography*, *21*(1), 68–81.
Large, W. G., and S. G. Yeager (2004), Diurnal to decadal global forcing for ocean and sea-ice models, *NCAR Tech. Note NCAR/TN-460+STR*, pp. 22, Natl. Cent. for Atmos. Res., Boulder, Colo.
Large, W. G., and G. Danabasoglu (2006), Attribution and impacts of upper ocean biases in CCSM3, *J. Clim.*, *19*, 2325–2346.
Locarnini, R. A., A. V. Mishonov, J. I. Antonov, T. P. Boyer, H. E. Garcia, O. K. Baranova, M. M. Zweng, and D. R. Johnson (2010), World Ocean Atlas, 2009, in *NOAA Atlas NESDIS 68*, vol. 1, edited by T. S. Levitus, U.S. Gov. Print. Off., Washington, D. C.
Lukas, R., and E. Lindstrom (1991), The mixed layer of the western equatorial Pacific Ocean, *J. Geophys. Res.*, *96*, 3343–3357.
Madec, G. (2008), NEMO ocean engine, *Note Pôle Modél. 27*, Inst. Pierre- Simon Laplace, Paris.
Marchesiello, P., J. C. McWilliams, and A. F. Shchepetkin (2001), Open boundary conditions for long-term integration of regional ocean models, *Ocean Modell.*, *3*, 1–20.
McCreary, J. P., P. J. Kundu, and R. L. Molinari (1993), A numerical investigation of dynamics, thermodynamics and mixed layer processes in the Indian Ocean, *Prog. Oceanogr.*, *31*, 181–244.
McCreary, J. P., W. Han, D. Shankar, and S. R. Shetye (1996), Dynamics of the East India Coastal Current: 2. Numerical solutions, *J. Geophys. Res.*, *101*, 13,993–14,010, doi:10.1029/96JC00560.
Mecklenburg, S., et al. (2012), ESA's soil moisture and ocean salinity mission: Mission performance and operations, *IEEE Trans. Geosci. Remote Sens.*, *50*(5), 1354–1366.
Mignot, J., C. de Boyer Montégut, A. Lazar, and S. Cravatte (2007), Control of salinity on the mixed layer depth in the world ocean: 2. Tropical areas, *J. Geophys. Res.*, *112*, C10010, doi:10.1029/2006JC003954.
Moum, J. N., A. Perlin, J. D. Nash, and M. J. McPhaden (2013), Seasonal sea surface cooling in the equatorial Pacific cold tongue controlled by ocean mixing, *Nature*, *500*, 64–67, doi:10.1038/nature12363.
Murthy, V. S. N., Y. V. B. Sarma, D. P. Rao, and C. S. Murthy (1992), Water characteristics, mixing and circulation in the Bay of Bengal during southwest monsoon, *J. Mar. Res.*, *50*, 207–228.
Neetu, S., M. Lengaigne, E. M. Vincent, J. Vialard, G. Madec, G. Samson, M. R. Ramesh Kumar, and F. Durand (2012), Influence of upper-ocean stratification on tropical cyclone-induced surface cooling in the Bay of Bengal, *J. Geophys. Res.*, *117*, C12020, doi:10.1029/2012JC008433.
Nidheesh, A. G., M. Lengaigne, J. Vialard, A. S. Unnikrishnan, and H. Dayan (2012), Decadal and long-term sea level variability in the tropical Indo-Pacific Ocean, *Clim. Dyn.*, *41*, 381–402.
Niiler, P. P., and E. B. Kraus (1977), One-dimensional models of the upper ocean, in *Modelling and Prediction of the Upper Layer of the Ocean*, edited by E. B. Kraus, pp. 143–172, Pergamon, Oxford, U. K.
Nisha, K., M. Lengaigne, V. V. Gopalakrishna, J. Vialard, S. Pous, A. C. Peter, F. Durand, and S. Naik (2013), Processes of summer intraseasonal sea surface temperature variability along the coasts of India, *Ocean Dyn.*, *63*, 329–346.
Nyadjro, E. S., B. Subrahmanyam, and J. F. Shriver (2011), Seasonal variability of salt transport during the Indian Ocean monsoons, *J. Geophys. Res.*, *116*, C08036, doi:10.1029/2011JC006993.
Papa, F., F. Durand, A. Rahman, S. K. Bala, and W. B. Rossow (2010), Satellite altimeter-derived monthly discharge of the Ganga-rahmaputra River and its seasonal to interannual variations from 1993 to 2008, *J. Geophys. Res.*, *115*, C12013, doi:10.1029/2009JC006075.
Parampil, S. R., A. Gera, M. Ravichandran, and D. Sengupta (2010), Intraseasonal response of mixed layer temperature and salinity in the Bay of Bengal to heat and freshwater flux, *J. Geophys. Res.*, *115*, C05002, doi:10.1029/2009JC005790.

Prasanna Kumar, S., P. M. Muraleedharan, T. G. Prasad, M. Gauns, N. Ramaiah, S. N. de Souza, S. Sardesai, and M. Madhupratap (2002), Why is the Bay of Bengal less productive during summer monsoon compared to the Arabian Sea?, *Geophys. Res. Lett.*, *29*(24), 2235, doi:10.1029/2002GL016013.

Praveen Kumar, B., J. Vialard, M. Lengaigne, V. S. N. Murty, G. R. Foltz, M. J. McPhaden, S. Pous, and C. de Boyer Montegut (2014), Processes of interannual mixed layer temperature variability in the thermocline ridge of the Indian Ocean, *Clim. Dyn.*, doi:10.1007/s00382-014-2059-y.

Rao, R. R., and R. Sivakumar (1999), On the possible mechanisms of the evolution of a mini-warm pool during the pre-summer monsoon season and the onset vortex in the southeastern Arabian Sea, *Q. J. R. Meteorol. Soc.*, *125*, 787–809.

Rao, R. R., and R. Sivakumar (2003), Seasonal variability of sea surface salinity and salt budget of the mixed layer of the north Indian Ocean, *J. Geophys. Res.*, *108*(C1), 3009, doi:10.1029/2001JC00907.

Schott, F., and J. P. McCreary (2001), The monsoon circulation of the Indian Ocean, *Prog. Oceanogr.*, *51*, 1–123, doi:10.1016/S0079–6611(01)00083-0.

Sengupta, D., G. N. Bharath Raj, and S. S. C. Shenoi (2006), Surface freshwater from Bay of Bengal runoff and Indonesian throughflow in the tropical Indian Ocean, *Geophys. Res. Lett.*, *33*, L22609, doi:10.1029/2006GL027573.

Sengupta, D., R. G. Bharath, and D. S. Anitha (2008), Cyclone-induced mixing does not cool SST in the post-monsoon north Bay of Bengal, *Atmos. Sci. Lett.*, *9*, 1–6, doi:10.1002/asl.162.

Seo, H., S. P. Xie, R. Murtugudde, M. Jochum, and A. J. Miller (2009), Seasonal effects of Indian Ocean freshwater forcing in a regional coupled model, *J. Clim.*, *22*, 6577–6596.

Shankar, D., J. P. McCreary, W. Han, and S. R. Shetye (1996), Dynamics of the East India Coastal Current 1. Analytic solutions forced by interior Ekman pumping and local alongshore winds, *J. Geophys. Res.*, *101*, 13,975–13,991, doi:10.1029/96JC00559.

Shankar, D., P. N. Vinayachandran, and A. S. Unnikrishnan (2002), The monsoon currents in the north Indian Ocean, *Prog. Oceanogr.*, *52*, 63–120, doi:10.1016/S0079–6611(02)00024-1.

Sharma, R., N. Agarwal, I. M. Momin, S. Basu, and V. K. Agarwal (2010), Simulated sea surface salinity variability in the tropical Indian Ocean, *J. Clim.*, *23*, 6542–6554, doi:10.1175/2010JCLI3721.1.

Shenoi, S. S. C. (2010), Intra-seasonal variability of the coastal currents around India: A review of the evidences from new observations, *Indian J. Mar. Sci.*, *39*(4), 489–496.

Shenoi, S. S. C., D. Shankar, and S. R. Shetye (1999), On the sea surface temperature high in the Lakshadweep Sea before the onset of the southwest monsoon, *J. Geophys. Res.*, *104*, 15,703–15,712.

Shenoi, S. S. C., D. Shankar, and S. R. Shetye (2002), Difference in heat budgets of the near-surface Arabian Sea and Bay of Bengal: Implications for the summer monsoon, *J. Geophys. Res.*, *107*(C6), 3052, doi:10.1029/2000JC000679.

Shetye, S. R. (1993), The movement and implications of the Ganges–Bramhaputra runoff on entering the Bay of Bengal, *Curr. Sci.*, *64*(1), 32–38.

Shetye, S. R., S. S. C. Shenoi, A. D. Gouveia, G. S. Michael, D. Sundar, and G. Nampoothiri (1991), Wind-driven coastal upwelling along the western boundary of the Bay of Bengal during the southwest monsoon, *Cont. Shelf Res.*, *11*, 1397–1408.

Shetye, S. R., A. D. Gouveia, D. Shankar, G. S.Michael, and G. Nampoothiri (1996), Hydrography and circulation of the western Bay of Bengal during the Northeast Monsoon, *J. Geophys. Res.*, *101*, 14,011–14,025.

Sudre, J., C. Maes, and V. Garçon (2013), On the global estimates of geostrophic and Ekman surface currents, *Limnol. Oceanogr.: Fluids Environ.*, *3*, 1–20, doi:10.1215/21573689-2071927.

Thadathil, P., V. V. Gopalakrishna, P. M. Muraleedharan, G. V. Reddy, N. Araligidad, and S. S. C. Shenoy (2002), Surface layer temperature inversion in the Bay of Bengal, *Deep Sea Res., Part I*, *49*, 1801–1818.

Thadathil, P., P. M. Muraleedharan, R. R. Rao, Y. K. Somayajulu, G. V. Reddy, and C. Revichandran (2007), Observed seasonal variability of barrier layer in the Bay of Bengal, *J. Geophys. Res.*, *112*, C02009, doi:10.1029/2006JC003651.

Uppala, S. M., et al. (2005), The ERA-40 re-analysis, *Q. J. R. Meteorol. Soc.*, *131*, 2961–3012, doi:10.1256/qj.04.176.

Vialard, J., K. Drushka, H. Bellenger, M. Lengaigne, S. Pous, and J. P. Duvel (2013), Understanding Madden-Julian-Induced sea surface temperature variations in the North Western Australian Basin, *Clim. Dyn.*, *41*, 3203–3218, doi:10.1007/s00382-012-1541-7..

Vincent, E. M., M. Lengaigne, J. Vialard, G. Madec, N. Jourdain, and S. Masson (2012), Assessing the oceanic control on the amplitude of sea surface cooling induced by tropical cyclones, *J. Geophys. Res.*, *117*, C05023, doi:10.1029/2011JC007705.

Vinayachandran, P. N., and J. Kurian (2007), Hydrographic observations and model simulation of the Bay of Bengal freshwater plume, *Deep Sea Res., Part I*, *54*, 471–486.

Vinayachandran, P. N., and R. S. Nanjundiah (2009), Indian Ocean sea surface salinity variations in a coupled model, *Clim. Dyn.*, *33*, 245–263. doi:10.1007/s00382-008-0511-6.

Vinayachandran, P. N., C. P. Neema, S. Mathew, and R. Remya (2012), Mechanisms of summer intraseasonal sea surface temperature oscillations in the Bay of Bengal, *J. Geophys. Res.*, *117*, C01005, doi:10.1029/2011JC007433.

Vinayachandran, P. N., D. Shankar, S. Vernekar, K. K. Sandeep, P. Amol, C. P. Neema, and A. Chatterjee (2013), A summer monsoon pump to keep the Bay of Bengal salty, *Geophys. Res. Lett.*, *40*, 1777–1782, doi:10.1002/grl.50274.

Webster, P. J., et al. (2002), The JASMINE pilot study, *Bull. Am. Meteorol. Soc.*, *83*, 1603–1630, doi:10.1175/BAMS-83-11-1603.

Wu, L., F. Wang, D. Yuan, and M. Cui (2007), Evolution of freshwater plumes and salinity fronts in the northern Bay of Bengal, *J. Geophys. Res.*, *112*, C08017, doi:10.1029/2005JC003308.

Xie, P., and P. A. Arkin (1997), Analyses of global monthly precipitation using gauge observations, satellite estimates, and numerical model predictions, *J. Clim.*, *9*, 840–858.

Yu, L., J. J. O'Brien, and J. Yang (1991), On the remote forcing of the circulation in the Bay of Bengal, *J. Geophys. Res.*, *96*, 20,449–20,454.

Yu, Z., and J. P. McCreary (2004), Assessing precipitation products in the Indian Ocean using an ocean model, *J. Geophys. Res.*, *109*, C05013, doi:10.1029/2003JC002106.

Zhang, Y. C., W. B. Rossow, A. A. Lacis, V. Oinas, and M. I. Mishchenko (2004), Calculation of radiative flux profiles from the surface to top-of-atmosphere based on ISCCP and other global datasets: Refinements of the radiative transfer model and the input data, *J. Geophys. Res.*, *109*, D19105, doi:10.1029/2003JD004457.